A COMBINED BOTTOM-HOLE PRESSURE CALCULATION PROCEDURE USING MULTIPHASE CORRELATIONS AND ARTIFICIAL NEURAL NETWORK MODELS

by

Xiaopeng (Roy) Li

A thesis submitted to the Faculty and the Board of Trustees of the Colorado School of Mines in partial fulfillment of the requirements for the degree of Master of Science (Petroleum Engineering).

Golden, Colorado

Date _____

Signed: _____
Xiaopeng (Roy) Li

Signed: _____
Dr. Jennifer L. Miskimins
Thesis Advisor

Golden, Colorado

Date _____

Signed: _____
Dr. William (Will) Fleckenstein
Adjunct Professor and Head
Department of Petroleum Engineering

ABSTRACT

Artificial neural network (ANN) techniques have been adopted to predict bottom-hole pressures and have proved to have better, or at a minimum equivalent prediction performance than conventional prediction methods such as multiphase correlations and mechanistic modeling. With the applied design, the use of ANN techniques can be more fully investigated to aid in multiphase flow related issues. In this study, different artificial neural network models have been trained to solve two of the major problems of bottom-hole pressure calculations - flow regime recognition and pressure gradient prediction.

A support vector machine model was trained for flow regime classification. In order to include inclination angle effects on flow regime transition, the model uses inclination angle and as well as gas and liquid velocity numbers as input variables. Four possible different flow patterns were considered for upward and horizontal multiphase flow, including bubble flow, slug flow, annular mist flow and stratified flow. Some 3-D plots of all the possible flow patterns at all inclination angles (from horizontal to upward vertical) within the studied condition range were generated based on model outputs.

Previous back-propagation neural network models in the literature have been modified to fit into piece-wise calculation procedures of multiphase correlations to achieve higher prediction accuracy and broaden the prediction range. The model training requires well-segment-scale data sets, which contain pressure gradients as the model output variable and the model input variables, including inclination angle, liquid superficial velocity, gas superficial velocity, gas-liquid surface tension, liquid density, specific gravity of free gas, liquid viscosity, gas viscosity, average pressure and average temperature. The training data was collected from literature and as well as some piece-wise calculation results of multiphase correlations. Different back-propagation neural network model structures have been tested to find a suitable neuron number on hidden-layer. Two pressure gradient prediction models

were trained for slug flow and annular mist flow.

Finally, a combined bottom-hole calculation procedure was designed based on multiphase correlations and trained artificial neural network models. The statistical test results using the collected data show that the combined procedure has the best prediction performance than the eleven multiphase correlations studied in this work with the lowest average absolute percent error of 3.1% and standard deviation of 0.034. Some independent field data was used to test the extendability of the combined procedure prediction range. Comparing to the multiphase correlations, the combined procedure gave fairly accurate predictions with an average absolute percent error of 23.0% and a standard deviation of 0.176. To facilitate field application, a multiphase flow bottom-hole pressure calculator with a user graphic interface was developed.

TABLE OF CONTENTS

LIST OF FIGURES

LIST OF TABLES

LIST OF SYMBOLS

d . . . . . Inner Diameter, in

g . . . . . , Gravitational Conversion Constant, $= 32.2\ (lbm/lbf) \cdot (ft/sec^2)$

MD . . . . . Measured Depth, ft

ΔMD . . . . . Well Segment Length, ft

ΔMD_0 . . . . . Assumed Well Segment Length, ft

N_{Lv} . . . . . Liquid Velocity Number, -

N_{gv} . . . . . Gas Velocity Number, -

N_d . . . . . Pipe Diameter Number, -

N_L . . . . . Liquid Viscosity Number, -

P . . . . . Pressure, $psia$

P_0 . . . . . Top Pressure of Well Segment, $psia$

ΔP . . . . . Pressure drop, psi

Δp_f . . . . . frictional pressure drop, psi

dP_T . . . . . Total Pressure Gradient, psi/ft

T . . . . . Temperature, F

T_0 . . . . . Top Temperature of Well Segment, F

v_{sL} . . . . . Liquid Superficial Velocity, ft/sec

v_{sg} . . . . . Gas Superficial Velocity, ft/sec

μ_L . . . . . Liquid Viscosity, cp

σ_L . . . . . Liquid-gas Surface Tension, $dynes/cm$

ρ_L . . . . . Liquid Density, lbm/ft^3

θ . . . . . Inclination Angle (from horizontal direction), $^\circ$

LIST OF ABBREVIATIONS

Artificial Neural Network	ANN
Barrel	bbl
Bottom-hole Pressure	BHP
Back-propagation	BP
Graphic-User-Interface	GUI
Inclination Angle	Inc
Plug-back Total Depth	PBTD
Standard Cubic Feet	scf
Specific Gravity	S. G.
Support Vector Machine	SVM

ACKNOWLEDGMENTS

The author wishes to express the deepest gratitude and appreciation to his advisor, Dr. Jennifer Miskimins, for the consistent, indispensable guidance and caring throughout the entire thesis work. Special thanks are due to Mr. Robert Sutton for his suggestions and shared knowledge during each communication, and Dr. Mark Miller for his input and comments on the thesis work.

Appreciation is extended to the Fracturing, Acidizing, Stimulation Technology (FAST) consortium for financially sponsoring this thesis work. This project would never have been possible without the support of the member companies in the FAST, especially Core Laboratories and Devon Energy Corporation for providing field data to this research. Dr. Todd Hoffman is greatly acknowledged for his support and encouragement since he became the Director of the FAST.

Special thanks to Ms. Denise Winn-Bower for her great help with the school registration and project progress. Thanks to Mr. Alireza Sami and Mr. Joe Chen for their encouragements during the author's thesis work. Good friends, like Wei Xu, Zhou Zhou, Yuan Liu and many more at Mines make the author feel great when they are around; the author's sincere thanks go to them.

Contributions of many fellow research workers in the area of multiphase flow and artificial neural network techniques are acknowledged through the references cited in this dissertation. The author is grateful to Chih-Chung Chang and Chih-Jen Lin for developing the LIBSVM software for users to utilize support vector machine techniques and Erich Hoover for writing the LyX thesis template to format the thesis.

To

my parents,

Xiaozhong Li and Shuxian Wu,

for their support, understanding and personal sacrifices throughout this undertaking.

To

my brother,

Xiaohe Li,

to inspire him to experience, learn and harvest in his life.

And also to

my beloved Han.

CHAPTER 1

INTRODUCTION

In industry applications, multiphase flow often exists, especially in the petroleum, chemical and nuclear industries. Problems related to multiphase flow have been extensively studied for decades due to its frequent occurrence and importance. During the decades, many approaches, both experimental and theoretical, have been made by the petroleum industry to try to understand multiphase flow in wells for production from the bottom-hole to the wellhead or transportation between the wellhead and gathering station or sale lines.

1.1 General Aspects of the Problem

One of the key issues of the research on multiphase flow in wells is how to calculate the pressure drop over a certain length. The flow rate of each phase, temperature, wellhead pressure, density (or gravity), pipe configuration of a production well are determined or readily measured at surface (usually at the separator), but bottom-hole pressure (BHP) is not and can change with those measurements or parameters. Therefore, an essential problem arises on how to calculate the bottom-hole pressure with any set of given or measurable input data. This problem is of significant importance to oil and gas production optimization. One of the main purpose of nodal analysis, which is one of the common production optimization methods, is tubing design. With the aid of the knowledge of how to estimate the pressure difference between the wellhead and bottom-hole, the design engineer can select the proper tubing at the proper time so that the tubing size is neither too large for the reservoir pressure to sustain the production rate nor too small to take advantage of high reservoir pressure, thus maximizing primary recovery.

As for single phase flow, the flow pressure gradient is easy to be dealt with using conservation equations and charts or equations, like the Moody diagram (Moody, 1944) and the Colebrook equation (Colebrook, 1939). However, most gas wells produce some liquid, such

as formation water or injected hydraulic fracturing fluids; and most oil wells produce oil with some gas in it. When two or more phases simultaneously exist in the pipes, the flow behaviors become much more complex to predict than a single liquid or gas phase flow. Depending on the physical forces and interactions acting on different phases, there can be various phase distributions in the pipes, known as flow pattern or flow regimes(Brill and Mukherjee, 1999). Because multiphase flow pressure gradients change significantly with different flow patterns, the prediction of the flow regime is usually the priority of multiphase flow pressure calculation. The increasing complexity of multiphase flow results in more uncertainties and lower accuracy of pressure drop predictions than with single phase flow. Pipe diameter, flow rates, inclination angle, temperature, fluid properties can all change along the flow conduit, and so will the surface tension acting on pipe walls, inertia and buoyancy. Moreover, different flow regimes can often be observed in one given production well or experimental flow line, if the variation of pressure and temperature is high enough. Hence, those issues associated with multiphase flow should draw attention to those engineers who attempt to solve the pressure gradient problem.

From a practical point of view, hydraulic fractured horizontal well technology has become a key method to unlock unconventional resources, especially tight gas reservoirs in the recent years. Most of the produced gas comes with some amount of water (or liquid condensate), which makes the flow in those wells multiphase flow. In most cases, however, the flowing bottom-hole pressure is not measured directly, but calculated from the measured surface pressure using multiphase flow correlations. Thus, to optimize well production, the design engineer is faced with the difficult task of predicting the pressure loss and gas-water phase distribution for gathering, pumping, and transporting the multiphase flow in both a vertical and horizontal geometry. Also, the desire to have accurate pressure gradient predictions can come from the use of production analysis techniques, which require accurate rate and bottom-hole pressure histories. Directional drilling technology with the associated tools enables drilling engineers to force the well trajectory to follow the path suggested by

geologists and reservoir engineers for the maximum wellbore-reservoir contact area or other purposes. To be compatible with curvilinear or more complex trajectories instead of just horizontal, vertical or straight, inclined systems have therefore become a concern in pressure gradient calculations. Several excellent multiphase correlations only concentrate on vertical or horizontal flow, and thus can lose accuracy when applied to inclined flow calculation. Prediction results will be wrong if the inclination angle effect is neglected. How to integrate existing multiphase correlations, which have inclination effects included, with complex trajectory should be considered as well.

Most of the correlations developed are very restricted in terms of handling a wide variety of data sets and work well only for certain conditions; therefore, choosing the right or best correlation among the plethora of correlations available for certain conditions is one of the key points for pressure gradient calculation. Choosing a wrong correlation could produce extremely large errors. Recently, the application of artificial neural networks (ANN) on the prediction of bottom-hole pressures provides an integrated approach for oil and gas well production. The results from some papers suggest a better BHP prediction performance of ANN than multiphase correlations. Given sufficient actual field data sets or lab measurements, the neural network can be trained to predict pressure values much closer to the measured values than those from the established correlations.

1.2 Thesis Objectives

The purpose of this work is to utilize existing multiphase correlations and artificial neural network techniques to develop a robust multiphase flow bottom-hole pressure calculation procedure. To achieve this goal, the objectives of this thesis work are listed as follows:

- Review common multiphase correlations and the application of artificial neural network techniques on bottom-hole pressure prediction;
- Collect experimental and field data sets from literature and producing oil and gas fields;

- Choose and build artificial neural network (ANN) models to improve the prediction ability and accuracy for flow regimes and pressure gradients;
- Incorporate these ANN models and existing multiphase correlations and develop bottom-hole pressure calculation procedures which can select the proper correlation or model to determine BHP under different conditions;
- Test each correlation and validate the developed procedures using actual data; and,
- Develop a windows application with Graphic-User-Interface (GUI) to implement all the methodologies for convenient field application.

1.3 Thesis Layout

Based on the objectives above, this thesis starts with a literature review of the existing multiphase correlations to understand their validity and applicability as the first part of Chapter 2. An brief introduction on ANN is also included in Chapter 2.

Chapter 3 describes how the flow regime map data was utilized to train a Support Vector Machine (SVM) model to classify flow regimes under certain conditions. With inclination angle effects included, some 3-D plots generated by the SVM prediction models are presented.

Chapter 4 is the key part of this thesis. Before introducing the BHP calculation procedure, the required petrophysical correlations are given here to estimate the fluid properties as intermediate variables to proceed the calculation. A detailed calculation procedure flow chart and description follows. To improve the prediction accuracy, back-propagation (BP) neural network models are brought into the calculation procedure. A brief demonstration on how to integrate BP neural network models with BHP calculations is also included. Finally, based on the literature review in Chapter 2 and the BP neural network approach, a robust combined BHP calculation procedure is developed and described.

In Chapter 5, the neural network model prediction performance is compared with multiphase correlations using the model training data. In order to expedite the testing process

and facilitate field application, a windows application is written in FORTRAN based on the statistical calculation results. Brief information on the application interface and instruction are given as well. Then some field data, which is completely independent of the training data, is introduced to validate the statistical results.

The purpose of Chapter 6 is to summarizes all the thesis work, illustrate the innovation and advantage of the methodology discussed, emphasize the critical issues, as well as point out the future potential or possible directions of this work. Chapter 7 lists all the major conclusions of this thesis work and some recommendations are also made here.

CHAPTER 2

BACKGROUND

Due to the complexity of inhomogeneous multiphase flow, no equations have been developed that can exactly describe the physical mechanisms or model multiphase systems. Early investigations into such systems started with correlations by plotting experimental or field data and fitting the resulting curves to equations of some form. Even later mechanistic modeling requires some empiricism to proceed with multiphase flow pressure calculations. This empiricism of multiphase correlations limits their pressure gradient prediction range to the flow conditions under which the correlations were developed. High prediction accuracy using one of these correlations is likely when the flow conditions are within the range, which was used to develop this particular correlation, unless the data sets have some errors in them. Therefore, to appropriately utilize multiphase correlations, it is important to understand the validity and applicability of each one of them. Section 2.1 describes eleven different multiphase correlations and their applicabilities.

Besides correlation and modeling approaches, Artificial Neural Network (ANN) techniques have been adopted by petroleum engineering researchers to solve pressure gradient issues in multiphase systems. A brief introduction to ANN and previous work using ANN to predict Bottom-hole Pressure (BHP) are included in Section 2.2.

2.1 Multiphase Flow Correlations

Brill and Mukherjee (1999) placed the empirical multiphase correlations into three categories:

Category A: No slip[1], no flow pattern considered. Gas and liquid phases are assumed to have the same flow velocity. The calculation procedure is the same for all flow

[1]Slip: normally, in gas-liquid flow, the gas phase travels faster than the liquid phase, and thus due to the slip between different phase velocities, two-phase flow cannot be treated as homogeneous flow.

patterns, which requires only one correlation to calculate the friction factor for the "homogeneous" gas-liquid mixture.

Category B: Slip considered, no flow pattern considered. Correlations are developed to calculate both liquid holdup[2] and friction factor and used for all flow patterns.

Category C: Both slip effect and flow pattern are considered. The flow pattern is predicted at first by using sets of equations of correlations, and then according to which flow pattern was predicted at the first step, corresponding different sets of equations are chosen to estimate liquid holdup and friction factor.

Eleven different correlations were chosen for this thesis study, which cover all three of the categories discussed above. Table 2.1 summarizes the correlations and the categories which they belong to:

Table 2.1: Multiphase Flow Correlations and Categories Summary

Correlation	Abbreviation	Category
Poettman and Carpenter (1952)	POECAR	a
Baxendell and Thomas (1961)	BAXTHO	a
Fancher and Brown (1963)	FANBRO	a
Hagedorn and Brown (1965)	HAGBRO	b
Gray (1978)	GRA	b
Dukler et al. (1969)	DUK	b
Duns and Ros (1963)	DUNROS	c
Orkiszewski (1967)	ORK	c
Beggs and Brill (1973)	BEGBRI	c
Mukherjee and Brill (1985)	MUKBRI	c
Aziz, Govier and Fogarasi (1972)	AZIZ	c

It should be noted that the statistical parameters used in this thesis work can be calculated by Equations 2.1, 2.2 and 2.3.

$$percent\ error = \frac{(Observed Values - Calculated Values)}{Observed Values} \times 100\% \tag{2.1}$$

[2]Liquid Holdup: the fraction of pipe occupied by liquid phase at any location.

$$absolute\,percent\;error = \frac{|Observed\,Values - Calculated\,Values|}{Observed\,Values} \times 100\% \tag{2.2}$$

$$standard\;deviation = \sqrt{\frac{N\sum_0^N (percent\,error)^2 - \left(\sum_0^N percent\,error\right)^2}{N^2}} \tag{2.3}$$

2.1.1 Poettman and Carpenter (1952) Correlation

Based on field data from 49 flowing and gas-lift wells, Poettman and Carpenter (1952) correlated the friction factor of multiphase flow with the product of the inside diameter of tubing and the mass velocity of the mixture flowing through the pipe. It should be noted that this dimensional product corresponds to the numerator of the Reynolds number.

2.1.2 Baxendell and Thomas (1961) Correlation

Due to the unsuccessful extrapolation of the Poettman and Carpenter correlation from low flow rates to high flow rates, Baxendell and Thomas (1961) suggested some modifications to the Poettman and Carpenter correlation to fit smoothly to the high-rate correlation derived from Cia, Shell de Venezuela's La Paz field in Venezuela.

2.1.3 Fancher and Brown (1963) Correlation

Fancher and Brown (1963) conducted a series of experiments on a 8000-ft experimental field well for flow rates ranging from 75 to 936 bbl/day at various gas-liquid ratios from 105 to 9433 scf/bbl. They found obvious deviation from the Poettman and Carpenter correlation for a certain range of flow rates and gas-liquid ratios. In order to fit the experimental data, they treated the gas-liquid ratio as an additional parameter and divided the range into three parts. For each range, a correlation was developed between friction factor and the numerator of the Reynolds number. The comparison of the three correlations in "Category a" from Table 2.1, i.e. Poettman and Carpenter (1952) correlation, Baxendell and Thomas (1961) correlation and Fancher and Brown (1963) correlation, is shown in Figure 2.1.

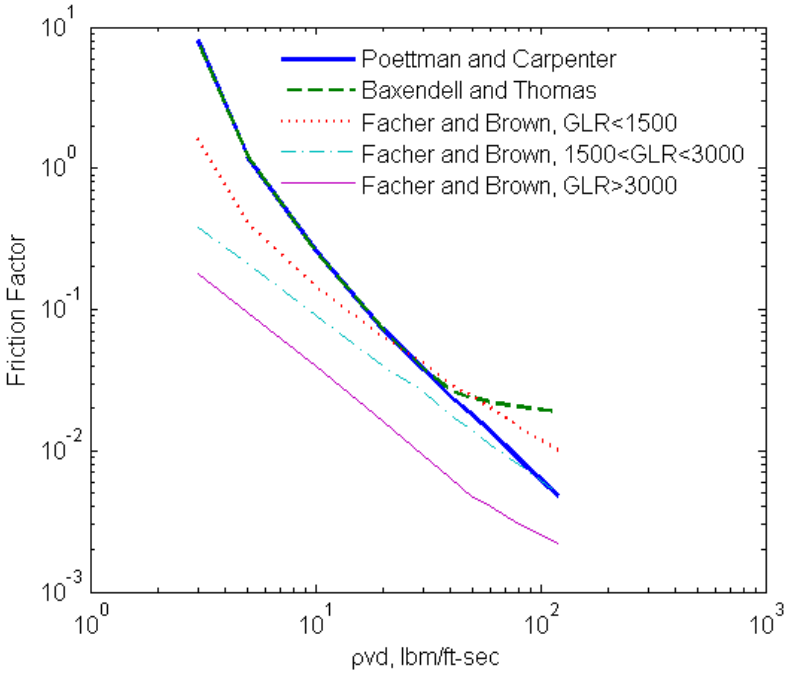

Figure 2.1: "Category a" friction factor correlations (Brill and Mukherjee, 1999). The three correlations plotted all used the numerator of the Reynolds number ρvd to predict friction factor. Baxendell and Thomas (1961) correlation modified Poettman and Carpenter (1952) correlation at high flow rates and Fancher and Brown (1963) correlation considered gas-liquid ratio as an additional parameter.

2.1.4 Hagedorn and Brown (1965) Correlation

Earlier approaches than the work by Hagedorn and Brown (1965) had been to correlate liquid holdup with known fluid, pipe and flow properties; the friction factor then could be calculated from the liquid holdup using experimental data. Hagedorn and Brown instead allowed a value of pseudo liquid holdup to perform friction factor calculations to estimate total pressure gradient at first. Then liquid holdup is calculated from the determined friction factor and test data. It should be noted that liquid holdup values in the liquid holdup correlation were calculated values instead of true measurements of the actual fraction of the pipe occupied by liquid.

The Hagedorn and Brown (1965) correlation involves only dimensionless groups proposed by Duns and Ros (1963), shown below, which is a condition usually sought for in similarity analysis but not always achieved. Additionally, correlations and equations satisfy the conditions when the flow rate of either gas phase or liquid phase reduces to zero, namely single phase flow.

Liquid velocity number,

$$N_{Lv} = v_{SL}\sqrt[4]{\frac{\rho_L}{g\sigma_L}} \tag{2.4}$$

Gas velocity number,

$$N_{gv} = v_{Sg}\sqrt[4]{\frac{\rho_L}{g\sigma_L}} \tag{2.5}$$

Pipe diameter number,

$$N_d = d\sqrt{\frac{\rho_L g}{\sigma_L}} \tag{2.6}$$

Liquid viscosity number,

$$N_L = \mu_L\sqrt[4]{\frac{g}{\rho_L\sigma_L^3}} \tag{2.7}$$

where, v_{sL} = Liquid Superficial Velocity, ft/sec;

ρ_L = Liquid Density, lbm/ft^3;

g = Gravitational Conversion Constant, $= 32.2\ (lbm/lbf) \cdot (ft/sec^2)$;

μ_L = Liquid Viscosity, cp;

σ_L = Liquid-gas Surface Tension, $dynes/cm$;

v_{sg} = Gas Superficial Velocity, ft/sec; and,

d = Inner Diameter, in.

The experimental data to develop this correlation was acquired under the following conditions:

- 1500-ft experimental vertical well;
- 1.0, 1.25, 1.5 in nominal diameter tubes;
- Liquids with different viscosities: 0.86 cp water, 30 cp oil, 35 cp oil, 110 cp oil;
- Liquid flow rates: 30-1680 bbl/day; and,
- Gas-liquid ratios: 0-3270 scf/bbl.

Hagedorn and Brown performed a statistical analysis on the results of the calculations utilizing the data obtained in their study as well as the data reported by Fancher and Brown (1963), Baxendell and Thomas (1961) and Gaither, Winkler and Kirkpatrick (1963) with a total average percent error of 1.101% and a total standard deviation of the percent errors of 6.469%.

2.1.5 Gray (1978) Correlation

This method takes the effects of liquids (condensate and/or free water) in gas well production into account for pressure gradient calculations and was developed especially for two-phase flow in *vertical* gas wells (Gray, 1978). It is recommended by the API in their manual for subsurface controlled safety valve sizing computer programs. The Gray correlation uses no-slip holdup and two dimensionless numbers, which are similar to the Velocity

Number and Pipe Diameter Number defined by Duns and Ros (1963), to calculate the liquid holdup.

A total of 108 selected well test data sets were used in developing this correlation, of which, 88 data sets were obtained from wells reported to produce free liquids. Additionally, another 65 data sets were randomly selected for statistical control purposes. Prediction results were compared to observations from both test and control data sets. The results were superior to the predictions made by conventional dry gas models and for pressure gradient prediction, the average bias is -0.35% and average standard deviation is 5.2% (Gray, 1978).

Yet, the accuracy was stated to be questionable when,

- Mixture velocity, $v_m > 50$ ft/sec;
- Pipe diameter, d > 3.5 in (nominal);
- Liquid condensate and gas ratio > 50 bbl/Mmscf; and,
- Water and gas ratio > 5 bbl/Mmscf.

2.1.6 Dukler et al. (1969) Correlation

In this thesis study, the Eaton, Knowles and Silberbrg (1967) correlation was used for liquid holdup calculations and the Flanigan (1958) correlation for elevational pressure gradient calculation. They were combined with the Dukler et al. (1969) correlation calculation procedure for horizontal flow pressure loss calculation.

For the Dukler et al. correlation, a total of approximately 400 *horizontal* flow experimental data points were utilized to established a graphical relationship between friction factor and Reynolds number, then friction pressure drop in two-phase flow would be calculated through similarity analysis approach (Dukler, Wicks and Cleveland, 1964). Liquid holdup was obtained through a trial and error calculation procedure (Dukler et al., 1969).

Data to develop the Eaton, Knowles and Silberbrg (1967) correlation were taken from a horizontal multiphase test unit, consisting of two 1700-ft test lines with diameters of 2 and

4 in. Flow condition ranges for the test are as follows (Eaton, Knowles and Silberbrg, 1967):

- Liquid rates: 50 to 2500 bbl/day for the 2-in line; 50 to 5500 bbl/day for the 4-in line.
- Gas-liquid ratio: 0 to 132000 scf/bbl for the 50 bbl/day liquid rate; a narrower range for the higher liquid rates.

The physical properties of test fluids can be summarized as,

- Gas: natural gas with S.G. (specific gravity) of 0.6111 and viscosity of 0.012 cp @ $80F$.
- Water: S.G. of 10.01, surface tension of 66.0 $dynes/cm$, viscosity of 1.01 cp @ $80F$.
- Crude: S.G. of 0.865, surface tension of 30.0 $dynes/cm$, viscosity of 13.50 cp @ $80F$.
- Distillate: S.G. of 0.77, surface tension of 26.0 $dynes/cm$, viscosity of 3.50 cp @ $80F$.

Based on studies of small amounts of condensate in gas lines, Flanigan (1958) developed a liquid holdup correlation to account for the hydrostatic pressure difference in upward inclined flow. The Flanigan correlation is utilized in this study to calculate the elevation part of total pressure gradient. As for downhill flow, the elevation gradient is neglected.

2.1.7 Duns and Ros (1963) Correlation

Based on extensive laboratory experiments, the Duns and Ros (1963) method is expected to be more general and applicable to the full range of field operating conditions, including tubing and annular flow for a wide range of oil and gas mixtures with varying water cuts. About 4000 two-phase flow tests, comprising some 20,000 data points, were carried out on a *vertical* string, consisting of an inflow section with a length between 98 and 198 ft, a 32.8 ft long measuring section and a 6.6 ft long outflow section (Ros, 1961). The test configurations and flow conditions can be summarized as below,

- Pipe diameters ranged from 1.26 to 5.6 in; outer diameter of annulus was 5.6 in and inner diameter ranged from 2.37 to 3.54 in.

- Fluids used in the tests (besides water):
  - Lubricating oil: density of 53.1 to 58.5 lbm/ft^3, surface tension of 28.1 to 33.8 $dynes/cm$ and viscosity of 5.62 to 315.8 cp.
  - Gas oil: density of 51.6 to 52.3 lbm/ft^3, surface tension of 27 to 28 $dynes/cm$ and viscosity of 3.312 to 4.101 cp.
  - Mineral spirit: density of 48.7 lbm/ft^3, surface tension of 24.5 $dynes/cm$ and viscosity of 0.96 cp.
- Liquid superficial velocity: 0 to 328.1 ft/sec; gas superficial velocity: 0 to 10.5 ft/sec.

Accuracy and applicability:

The validity of the correlation was divided into three regions (Duns and Ros, 1963),

- Region 1: liquid phase is the continuous phase
  - Bubble flow, plug flow and part of froth-flow regime;
  - Standard deviation of the per cent errors is 3% for dry oil and gas mixtures, which is equal to the measuring accuracy.
- Region 2: phases of liquid and gas alternate
  - Slug flow and the rest of froth-flow regime;
  - Standard deviation of 8% for dry oil and gas mixtures.
- Region 3: gas phase is continuous
  - Mist flow;
  - Standard deviation of 6% after refinements.
- The discrepancy can amount to up to 10% in Region 1 and Region 2 with wet mixtures containing less than 10% of water.

2.1.8 Orkiszewski (1967) Correlation

Orkiszewski (1967) tested several existing correlations and found none of them proved accurate over the entire range of conditions of available data. He then presented this correlation for *vertical* two-phase flow, which is an extension of the Griffith and Wallis (1961) correlation. A new correlation for slug flow regime was developed using Hagedorn and Brown (1965) experimental data, and the Griffith and Wallis method was selected for bubble flow regime and Duns and Ros correlation was chosen to deal with mist flow regime.

The pressure drop prediction precision of this method was verified by comparison against 148 measured pressure drops,

- Standard deviation about 10.0% for two-phase pressure drop prediction in flowing and gas-lift production vertical wells over a wide range of well conditions;
- Four flow regimes were considered: bubble, slug, annular-slug transition, and annular mist; and,
- Unlike most other methods, liquid holdup was derived from observed physical phenomena.

2.1.9 Beggs and Brill (1973) Correlation

An experimental apparatus was designed and built to investigate the effect of pipe inclination angle on liquid holdup and pressure loss of gas-liquid flow in inclined pipes (Beggs and Brill, 1973). A total of 584 average liquid holdup and pressure drop measurements, from which this correlation was developed, were taken in transparent acrylic pipes, which could be inclined at any angle from the horizontal. The parameters studied and their range of variation were,

- Gas (air) flow rate: 0 to 300 $Mscf/day$;
- Liquid (water) flow rate: 0 to 1029 bbl/day;

- Average system pressure: 35 to 95 $psia$;
- Pipe diameter: 1.0 to 1.5 in;
- Liquid holdup: 0 to 0.870;
- Pressure gradient: 0 to 0.80 psi/ft;
- Inclination angle: -90° to +90°; and,
- Different flow patterns were observed.

Accuracy and applicability,

- Comparing with all the tests results, average percent error for liquid holdup prediction was -0.28% with a standard deviation of 7.89%. And for the pressure gradient prediction, the values were 1.11% and 9.30%;
- Based on air-water and small diameter pipe;
- Valid for all inclination angles;
- Only consider horizontal flow patterns; and,
- Inclination angle correction made for each flow pattern.

2.1.10 Mukherjee and Brill (1985) Correlation

For this experimental work, each leg of the U-shape test section was 56 ft long with 22 ft entrance lengths followed by 32 ft long test sections to simulate both uphill and downhill flow at the angle of 0° to ±90° from horizontal (Mukherjee and Brill, 1985). The fluids used were air-Kerosene or air-lube oil. During the test, each liquid flow rate was set at first, and then a series of different gas flow rates were introduced. For each gas and liquid flow rate, flow patterns were observed and holdup recorders and pressure gauges were activated. Approximately 1000 pressure-drop measurements and more than 1500 liquid holdup measurements were taken for a broad range of gas and liquid flow rates (Brill and Mukherjee, 1999).

Pressure loss calculation results from this method were compared with the observed horizontal and upward flow data (air-Kerosene only) with an average percent error of -0.422% and a standard deviation of 17.75% (Mukherjee, 1979). In addition, pressure loss predictions were compared with 14 pipeline data from Prudhoe Bay Field (horizontal flow) and 130 offshore well data from North Sea data (vertical flow) with average percent errors of -9.5% and -3.3%, and standard deviations of 14.67% and 9.7%, respectively.

2.1.11 Aziz, Govier and Fogarasi (1972) Correlation

Based on flow mechanism instead of experiment or field data, Aziz, Govier and Fogarasi (1972) proposed a pressure drop calculation scheme, which can be seen as a precursor of modern mechanistic models. Transition criteria and pressure gradient correlations for bubble, slug, froth (transition), annular mist flow regimes were described.

Field data from 48 wells were used to measure the accuracy of the proposed method. The calculation results were compared with other methods and the absolute error was about the same as the Orkiszewski (1967) method but more favorable than the Hagedorn and Brown (1965) and Duns and Ros (1963) methods.

2.2 Artificial Neural Network (ANN) Techniques

The human brain's memory is stored in the biological neurons and the connections between them, namely a biological neural network, and the learning process is viewed as an establishment of new connections or modification of existing connections (Hagan, Demuth and Beale, 1996). Scientists try to understand these biological neural functions and then construct a small set of artificial neurons to perform some certain useful functionality. Inspired by the structures and connections of biological neural networks, mathematical language was used to simulate the process in human brains. An artificial neural network is like a mathematical model, which can be used to map the model input data to the model output data, or to group data into different categories based on similarity criteria, etc.

2.2.1 Introduction to ANN Methods

So far, various artificial neural network models have been developed for different distinct purposes and applied in different areas to solve difficult tasks that cannot be dealt with using conventional methods. These ANN models include Back Propagation (BP) Neural Network for nonlinear fitting, Principal Component Analysis (PCA) Neural Network for feature extraction and dimension reduction, Support Vector Machine (SVM) Neural Network for pattern recognition, and Self Organizing Map (SOM) Neural Network for data clustering.

To illustrate the training or modeling process of artificial neural networks, one of the commonly used artificial neural networks, the BP neural network, is shown as an example here. Additionally, in order to demonstrate the applicability of this type of ANN to bottom-hole pressure calculation problems, some related variables and processes are also included in the example.

The BP neural network is well-known for its ability to recognize or model very complex relations between input and output data. The pressure and liquid holdup variations along pipe in multiphase flow is one of the fitted situations. A schematic of a simple BP neural network is shown in Figure 2.2, consisting of three parts, an input layer, a hidden layer in the middle, and an output layer. Each layer comprises some neurons linked to the neurons in the other layers.

The way to make an artificial neural network model work is through a training process. Take the bottom-hole pressure calculation as an example, at first, some input data are introduced to the input layer of neural network, such as inclination angles, gas and liquid flow rates, liquid viscosities, temperatures, wellhead pressure, and well length. Then the neurons in each layer, multiplied by the corresponding weights, are passed through a function called the activation function, such as a linear function, a hyperbolic tangent sigmoid function, to the next layer. Finally, the simulation BHP result is obtained from the output layer, which is different from the actual BHP data. Based on how close the ANN output is to the actual BHP data, the weights are adjusted and modified until the simulation result equals

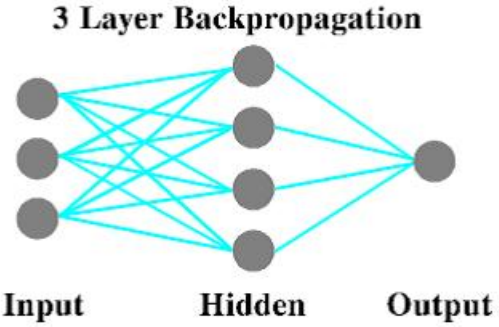

Figure 2.2: A schematic of a three-layer back propagation neural network from Ternyik et al. (1995). This neural network model has only one hidden layer, and the neuron number distribution on the three layers is 3-4-1.

the expected actual BHP value. After that, the neural network will use the "knowledge" it learns from the training process, i.e. the weights and the threshold values of each neuron, to respond to new input data by outputting an estimated BHP.

2.2.2 Applications in the Petroleum Industry

Because of the powerful ability to handle complicated implicit relationships and the versatility for multiple purposes of artificial neural network techniques, more and more efforts have been made by engineers and researchers in the petroleum industry to adopt this "new" methodology to solve various problems.

Ternyik et al. (1995) introduced ANN techniques to multiphase flow BHP prediction and developed a BP artificial neural network model based on the experimental data from Mukherjee. The applicability and advantages of the neural network model was successfully demonstrated.

Shippen and Scott (2002) developed a three-layer BP neural network model to predict liquid holdup in two-phase horizontal flow. A total of 627 holdup measurements were used to train the model. No flow regime effect was considered. Based on the extensive experimental and theoretical work by Ros (1961) and preliminary sensitivity analysis, several variables

were ruled out as input variables for the neural network model. The remaining variables for the input layer of the model are pipe diameter, gas and liquid superficial velocities, liquid viscosity, liquid density, and liquid surface tension. The comparison results with correlations and mechanistic models showed that the neural network model prediction performance was superior across the range of liquid holdup and was more consistent in terms of independence on liquid holdup range.

Osman (2004) built two three-layer BP neural network models to identify flow regimes and predict liquid holdup in horizontal multiphase flow based on 199 experimental data sets. The results indicated that the liquid holdup model outperformed all the existing horizontal multiphase correlations used for comparison and that the flow regime model classified different flow regimes correctly with more than 97% of the data points with high accuracy. After this work, Osman, Ayoub and Aggour (2005) built another neural network model to predict bottom-hole flowing pressure in vertical multiphase flow. The model consisted of one input layer, tree hidden (middle) layers, and one output layer after a series of optimization process by monitoring the performances of network models with different structures. Again, comparing with existing correlations and mechanistic models, the neural network model achieved the highest correlation coefficient and lowest average absolute percent error, lowest standard deviation, lowest maximum error, and lowest root mean square error.

Ozbayoglu and Ozbayoglu (2007) presented approaches to estimate frictional pressure loss and flow pattern of two-phase fluids flowing through horizontal annular geometries using different types of ANN models with different structures. ANN models considered in the study were BP neural network, Generalized Feed Forward neural network, Modular neural network, Principle Component Analysis neural network, Radial Basis Function neural network and Self Organizing Map neural network. Based on the prediction performance, the best ANN models were determined to predict pressure loss and flow pattern. The results showed that ANN models could estimate flow patterns with an error of less than 5% and frictional pressure losses with an error of less than 30%.

Mohammadpoor et al. (2010) trained several ANN models to predict bottom-hole flowing pressure in vertical multiphase flow in Iranian oil fields. Input data and output data were gathered from selected southern Iranian fields and were filtered to eliminate unreliable data and ensure the validity of the data. Models with varying number of neurons at hidden layer and activation functions were tested and the best one with the least error was chosen. The developed ANN models improved prediction accuracy by five times as compared with existing correlations.

To solve two phase annular flow pressure loss problems during under-balance drilling operations, Ashena et al. (2010) applied several BP neural network models with different network structures on two major Iranian oil fields. Through statistical analysis, they found that the trained BP neural network models performed much better in bottom-hole circulating pressure calculations than one mechanistic model, which was popularly used for these two fields.

Al-Shammari (2011) applied the Fuzzy Logic technique, one of the most famous Artificial Intelligence techniques, on bottom-hole pressure estimation and developed an Adaptive Neuron Fuzzy Inference System (ANFIS) model based on 596 well testing data. Flowing bottom-hole pressure was successfully predicted for 199 well testing samples with an average absolute error of 4.9%. The ANN model prediction achieved higher accuracy than all the flow correlations included in the study.

To conclude, recent developments of artificial neural network techniques on multiphase flow related problems, such as pressure drop, liquid holdup and flow pattern predictions, all show promising potential and superior performance than conventional methods such as correlations and mechanistic models.

CHAPTER 3

MULTIPHASE FLOW PATTERN CLASSIFICATION

As discussed in Section 2.1, flow pattern is one criterion to determine in which category a multiphase correlation belongs to. Flow pattern is one of the most important characteristics of multiphase flow as it distinguishes itself from single phase flow and also reflects the complexity of the multiphase system. Thus, any attempt to deal with multiphase flow in such a way similar to how single phase flow is treated will probably fail. Flow regime effects are crucial to the success of multiphase flow pressure gradient estimation and a necessity for an accurate multiphase correlation or mechanistic model.

Some recognized flow patterns for upward vertical flow include: bubble flow, slug flow, annular mist flow and the transition region between slug flow and annular mist flow. When multiphase flow starts to transit between different regimes, the pressure loss mechanism changes significantly due to phase distribution change. For example, bubble flow is characterized as where a gas phase exists in discrete bubbles and is uniformly distributed in a continuous liquid phase; whereas annular flow features the gas phase in the axial center of pipe with some liquid flowing upwards while leaving the rest of the liquid as a thin film around the pipe. Hence, the frictional pressure loss of bubble flow depends mostly on the shear stress between the liquid and pipe wall, while for annular mist flow, it is important to study the shear stress acting at the interface between the central gas core and the liquid film.

3.1 Flow Pattern Maps

Previous investigations on flow pattern prediction have focused on flow pattern maps. There is a wide range of possible flow regimes and each flow pattern can exist under various sets of conditions. Many names have been given to different flow regimes Brill and Beggs (1979).

Generally, to develop a flow pattern map, experimental data with visual observations of flow patterns were plotted with the chosen coordinates which were believed to best present different flow regimes. The commonly used coordinates are gas superficial velocity and liquid superficial velocity, gas velocity number and liquid velocity number. Not only are these coordinates used on flow pattern maps, but also to predict friction factor or other parameters in some correlations. The condition sets for each flow pattern in reality are believed to be continuous, in another words, the area of each flow regime on the map are plotted continuously and are not discrete. Thus, arises the problem of how to describe the transition boundaries. Based on experimental observations, smooth curves are generally drawn between different flow regimes to represent the boundaries. Then linear equations or equations of other forms are fitted to these drawn boundaries and used as transition criteria.

3.1.1 Vertical Flow Pattern Maps

For vertical flow, there is the Duns and Ros (1963) flow pattern map, shown in Figure 3.1. They proposed Equations 3.1-3.3 as flow pattern transition boundaries for Figure 3.1 (Brill and Mukherjee, 1999):

Bubble/slug boundary:

$$N_{gv} = L_1 + L_2 N_{Lv} \tag{3.1}$$

where, $L_1$and L_2 are functions of N_d.

Slug/transition boundary:

$$N_{gv} = 50 + 36 N_{Lv} \tag{3.2}$$

Transition/mist boundary:

$$N_{gv} = 75 + 84 N_{Lv}^{0.75} \tag{3.3}$$

where, N_{gv} = Gas Velocity Number, $-$;

N_{Lv} = Liquid Velocity Number, $-$; and,

N_d = Pipe Diameter Number, $-$.

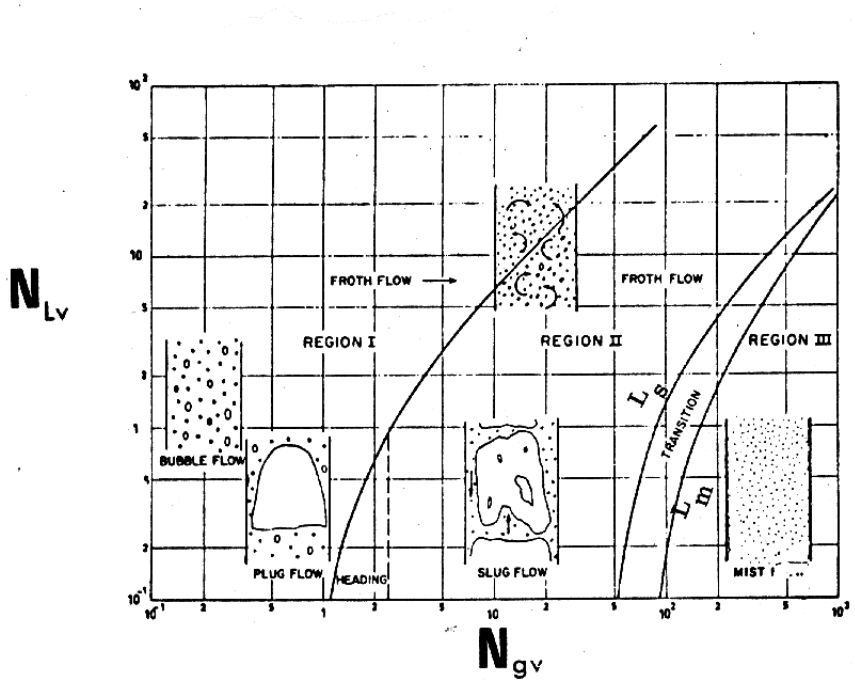

Figure 3.1: The Duns and Ros (1963) flow pattern map. Flow pattern data was plotted using liquid and gas velocity numbers as coordinates. Three regions, i.e. Region I, II, III, and a transition region were divided on this vertical flow pattern map by three boundary curves described by Equation 3.1-3.3.

Orkiszewski (1967) used the Duns and Ros flow pattern transition equations except bubble flow and slug flow boundary, for which he used the criteria by Griffith and Wallis (1961).

Aziz, Govier and Fogarasi (1972) used the flow pattern map shown in Figure 3.2, which was first presented by Govier, Sullivan and Wood (1961). The coordinates used are defined as,

Modified superficial gas velocity (ft/sec),

$$X = v_{sg}\left(\frac{\rho_g}{0.0764}\right)^{1/3}\left[\left(\frac{72}{\sigma_L}\right)\left(\frac{\rho_L}{62.4}\right)\right]^{1/4} \tag{3.4}$$

Modified superficial liquid velocity (ft/sec),

$$Y = v_{sL}\left[\left(\frac{72}{\sigma_L}\right)\left(\frac{\rho_L}{62.4}\right)\right]^{1/4} \tag{3.5}$$

where, v_{sg} = Gas Superficial Velocity, ft/sec;

ρ_L = Liquid Density, lbm/ft^3;

ρ_g = Gas Density, lbm/ft^3;

σ_L = Liquid-gas Surface Tension, $dynes/cm$; and,

v_{sL} = Liquid Superficial Velocity, ft/sec.

3.1.2 Horizontal Flow Patterns

Horizontal flow regimes are more difficult to predict than vertical flow, because the phases tend to segregate due to gravity effects and form stratified flow, which does not happen in vertical flow settings.

Beggs and Brill (1973) considered three different types of horizontal flow patterns, segregated flow, intermittent flow, distributed flow, as shown in Figure 3.3. They plotted a horizontal flow pattern map and then modified it to include a transition area between segregated flow and intermittent flow as shown in Figure 3.4 Brill and Beggs (1979). The dashed lines represent the modified boundaries, which were then correlated with input liquid content λ_L (or no-slip liquid holdup) and Froude number N_{Fr}, defined by Eq. 3.6,

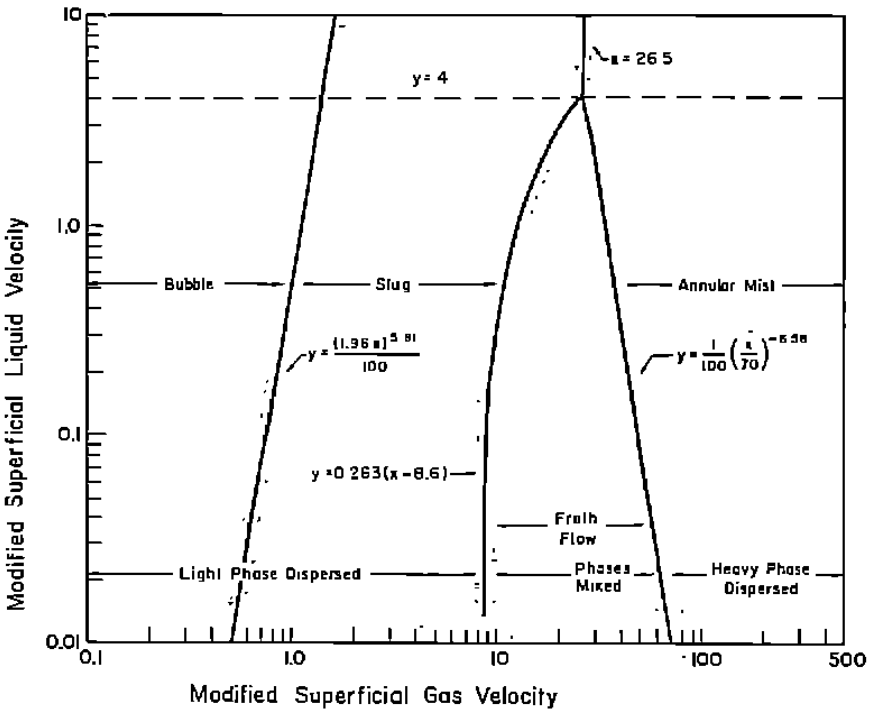

Figure 3.2: The Aziz, Govier and Fogarasi (1972) flow pattern map, first presented by Govier, Sullivan and Wood (1961), uses modified superficial gas and liquid velocity numbers, defined by Equation 3.4 and Equation 3.5, as coordinates. Four flow regimes are included, bubble flow, slug flow, froth (transition) flow and annular mist flow.

$$N_{Fr} = \frac{v_m^2}{gd} \tag{3.6}$$

where, v_m = Mixture Superficial Velocity, ft/sec;

g = Gravitational Conversion Constant, $= 32.2\ (lbm/lbf) \cdot (ft/sec^2)$; and,

d = Inner Diameter, in.

It should be noted that the flow pattern transition criteria equations determine the flow patterns that would exist if the flow was horizontal. Thus, this flow pattern map does not represent what the actual flow pattern is, unless the actual flow is horizontal.

Mandhane, Gregory and Aziz (1974) generated a flow pattern map (see Figure 3.5) as a log-log plot of superficial gas and liquid velocities. The map was based on a total of 5935 individual observations for horizontal flow from the University of Calgary's Multiphase Pipe Flow Data Bank. Six different flow patterns, including stratified flow, wave flow, bubble flow, slug flow, dispersed flow, annular flow, are presented on the map.

3.1.3 Inclined Flow Pattern Maps

So far, the inclination angle has not been considered in flow pattern transition criteria; and how to predict flow patterns within the full range of inclination angles from 0° to 90° from horizontal is of importance for inclined wells or even more, curved wells. The discontinuity of the types of flow patterns in vertical and horizontal flows should also be noted.

Gould, Tek and Katz (1974) studied the effect of pipe inclination on flow regimes. The results of direct observations from a two-phase flow apparatus were drawn in flow regime maps in Figure 3.6. A comparison of the maps in Figure 3.6(a), Figure 3.6(b) and Figure 3.6(c) leads to the conclusion that the liquid-phase-continuous area and gas-phase-continuous area do not vary significantly with pipe inclination angle.

Mukherjee (1979) conducted an extensive experimental study of inclined patterns in his thesis. Flow pattern maps were draw on log-log scales for different inclination angles with gas and liquid velocity numbers as coordinates, as shown in Figure 3.7. The imposed transition

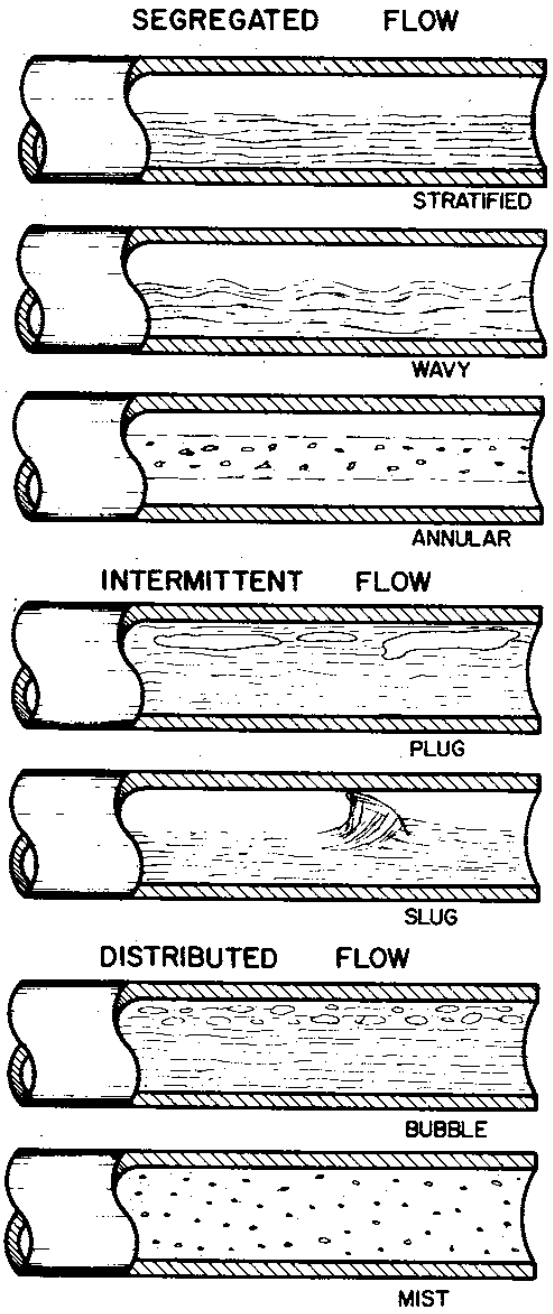

Figure 3.3: Beggs and Brill (1973) classified horizontal flow patterns into three different types based on the phases distribution, including segregated flow type (stratified flow, wavy flow, annular flow), intermittent flow type (plug flow, slug flow) and distributed flow type (bubble flow, mist flow).

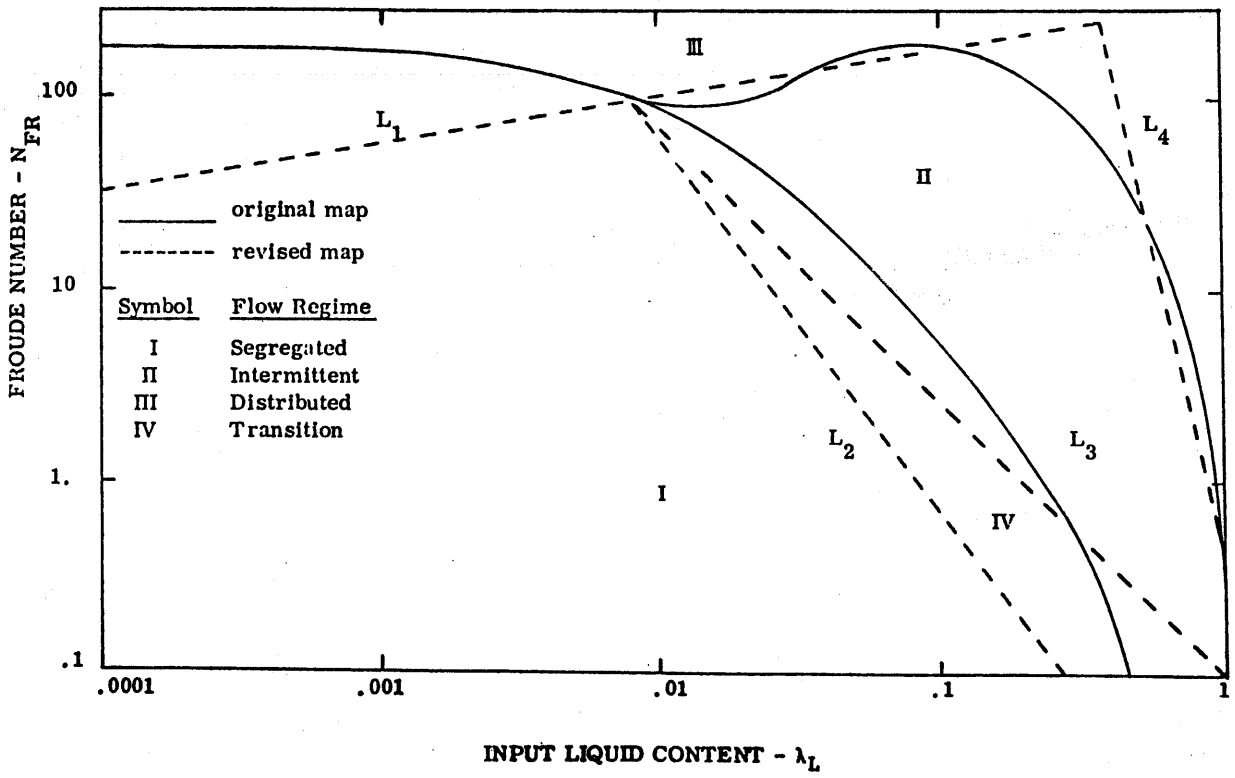

Figure 3.4: Beggs and Brill (1973) horizontal flow pattern map uses input liquid content and Froude number to determine flow pattern. The solid lines represent original transition boundaries and then were modified to include IV Transition Regime as shown by dashed lines.

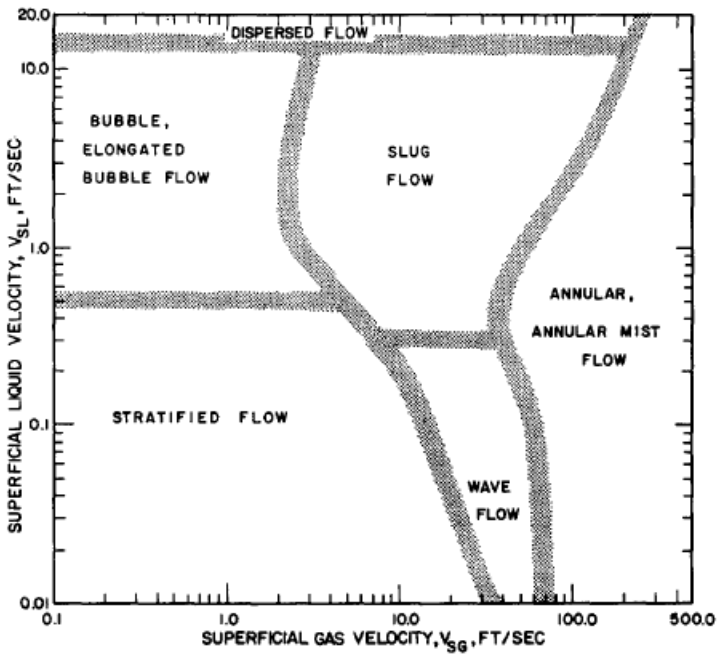

Figure 3.5: Mandhane, Gregory and Aziz (1974) horizontal flow pattern map presents six horizontal flow patterns using superficial gas and liquid velocities as coordinates, including bubble and elongated bubble flow, stratified flow, wave flow, slug flow, annular and annular mist flow, and dispersed flow.

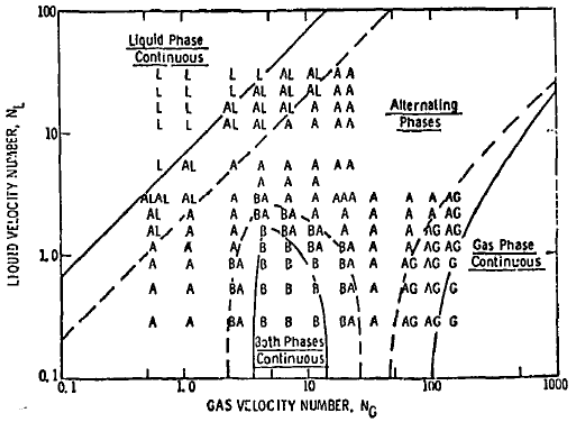

(a) Flow Regime Map, Vertical

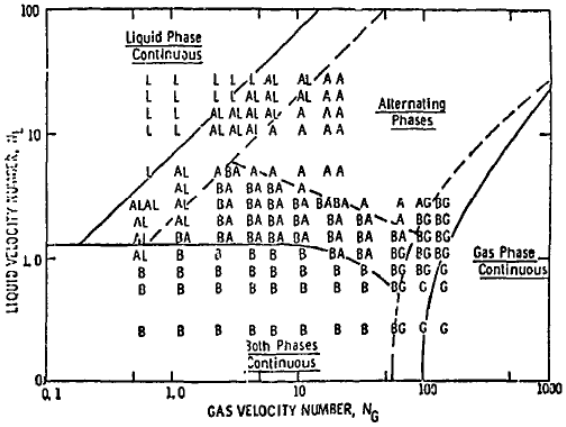

(b) Flow Regime Map, Horizontal

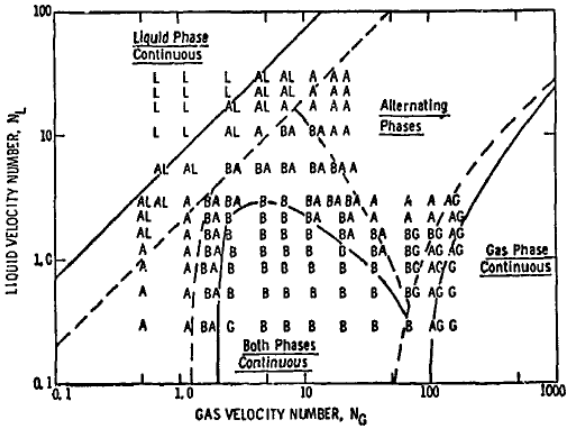

(c) Flow Regime Map, 45° from Horizontal

Figure 3.6: Gould, Tek and Katz (1974) flow regime map classifies flow regimes based on the continuous phase, including liquid-phase-continuous (L), gas-phase-continuous (G), alternating-phases (A), both-phases-continuous (B), and the transition regions between different flow regimes. By comparing the flow maps with different inclination angles in Figure 3.6(a), Figure 3.6(b), and Figure 3.6(c), they found the liquid-phase-continuous and gas-phase continuous flow regime boundaries do not appear to vary significantly with inclination.

curves on Figure 3.7(a), Figure 3.7(b), Figure 3.7(c) and Figure 3.7(d) were fitted with nonlinear regression equations.

Instead of empirically locating flow regime transition boundaries, Taitel, Bornea and Dukler (1980) proposed the basic physical mechanisms for each transition in vertical tubes. Barnea, Shoham and Taitel (1982) extended the limitations of Taitel, Bornea and Dukler flow regime transition models to inclined wells. Then Barnea (1987) combined the existing flow pattern transition models into a unified model. The transition boundaries predicted by this unified model were compared with the experimental data by Shoham (1982) for the whole range of pipe inclinations (see Figure 3.8). Maps were plotted on log-log scales and used superficial gas and liquid velocities (m/sec) as coordinates. A satisfactory agreement between theory predicted results and experimental observations was achieved.

3.2 Support Vector Machine Model

As part of this research, a Support Vector Machine (SVM) model was trained to recognize different flow patterns in horizontal and upwards flow.

3.2.1 Introduction

Support Vector Machine or Support Vector Networks theories were originally developed by Vapnik (1995) and proposed by Cortes and Vapnik (1995). To be exact, a Support Vector Machine (SVM) is actually a supervised learning method, such as the Back Propagation method. SVM models utilize similar structures to common Artificial Neural Network (ANN) models. In this study, the SVM model is considered to be an ANN model. Popular uses for SVM models are pattern classification and nonlinear regression. The learning process of the SVM model takes the training data to higher dimensional space, thus to avoid non-linearity of low dimensional space. Even if only limited training samples are provided, a SVM model can find a maximal separating hyperplane that can maximize its distances to training data in high dimensional feature space to ensure generalization and global optima. Based on statistical learning theories, the SVM method seeks to minimize the Structural

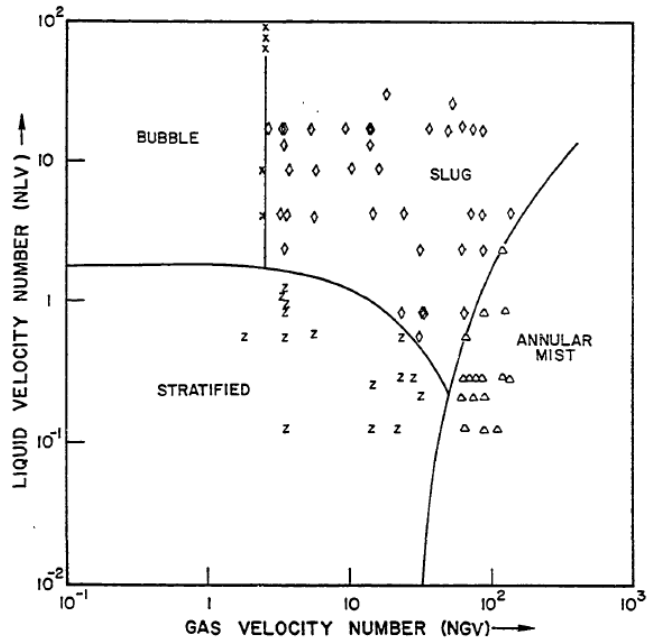

(a) Flow Pattern Map, Horizontal

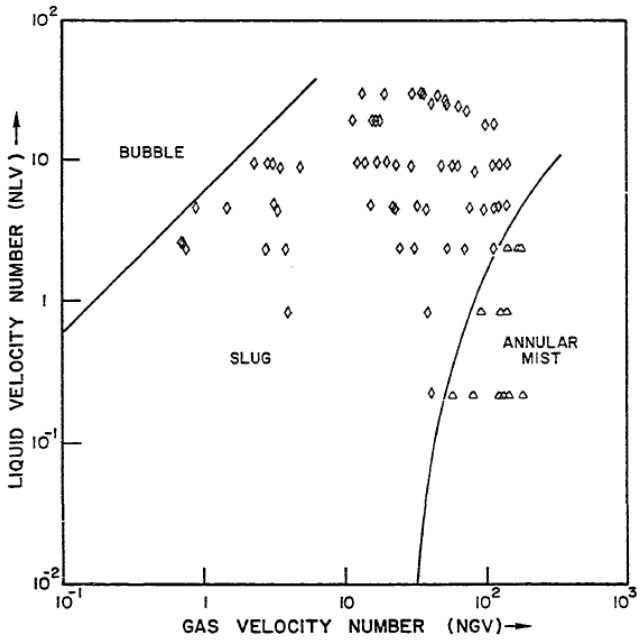

(b) Flow Pattern Map, 30° from Horizontal

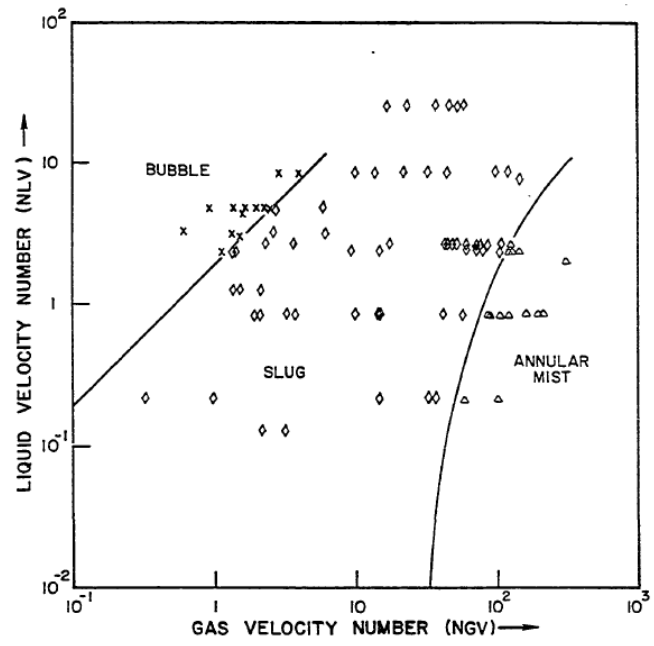

(c) Flow Pattern Map, 70° from Horizontal

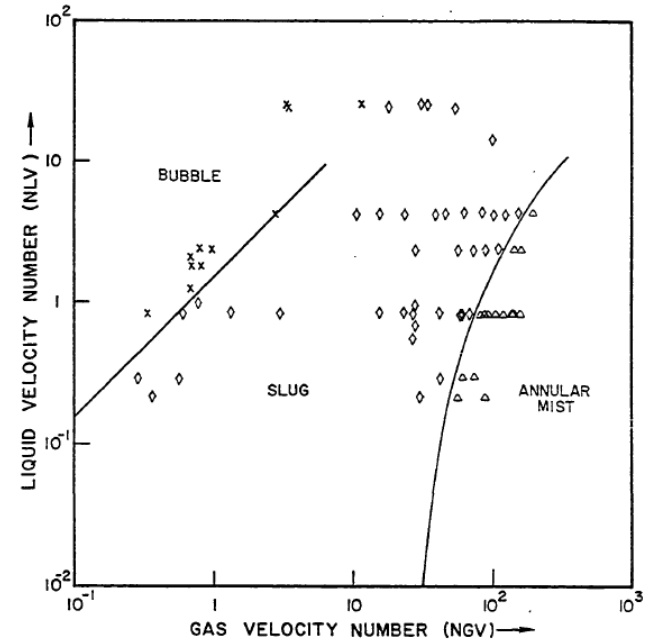

(d) Flow Pattern Map, Vertical

Figure 3.7: Mukherjee and Brill (1985) flow pattern maps. Experimental observations at different inclination angles (0°, 30°, 70°, 90° from horizontal) are plotted on log-log coordinates of gas and liquid velocity numbers in Figure 3.7(a), Figure 3.7(b), Figure 3.7(c), and Figure 3.7(d) (bubble flow as cross, slug flow as diamond, stratified flow as letter "z", annular mist flow as triangle). Solid transition boundaries are drawn and then correlated with regression equations. We can see that the transition boundaries do vary as inclination angle changes.

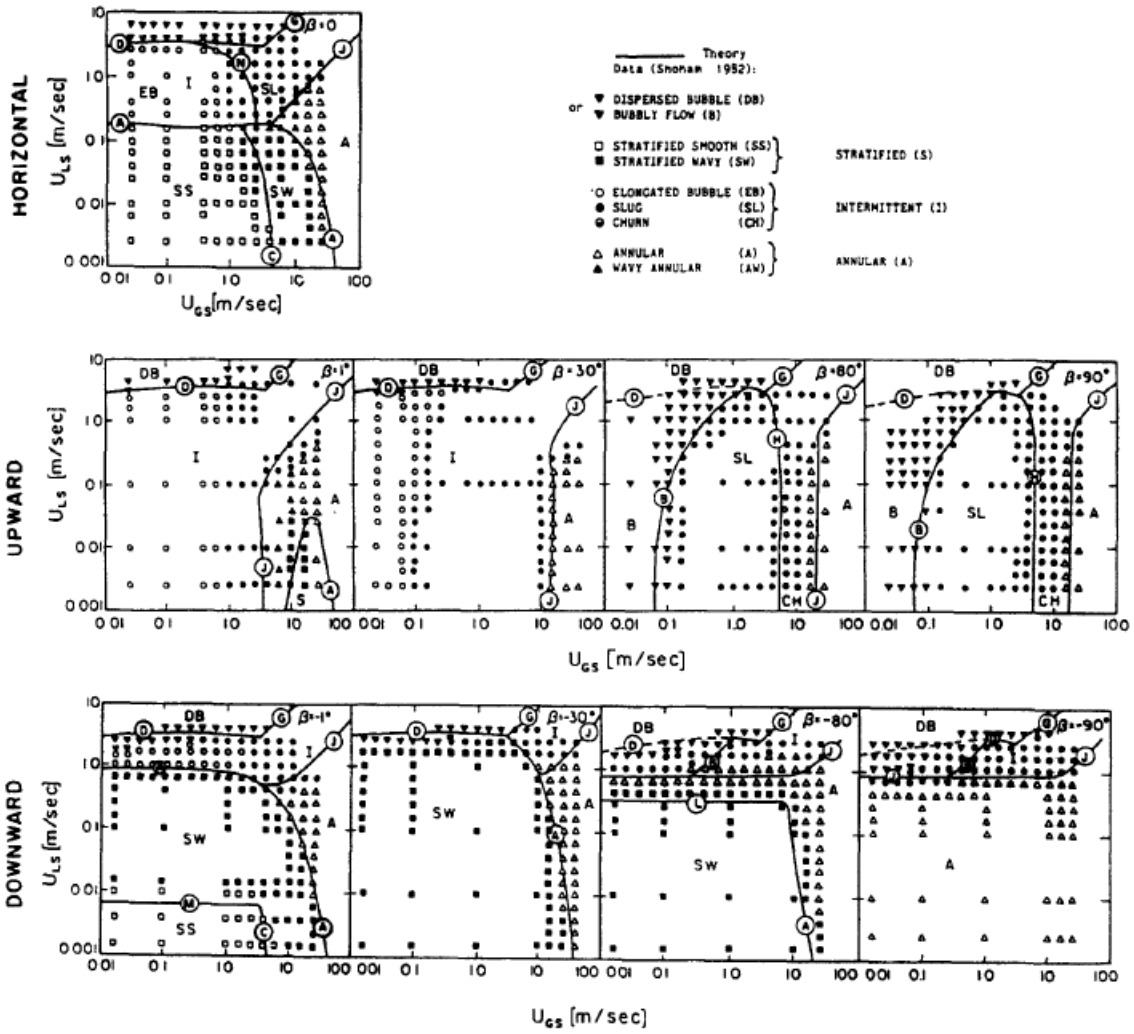

Figure 3.8: Barnea (1987) flow pattern maps for the whole range of inclinations, including horizontal flow, upward flow (1°, 30°, 80°, 90° from horizontal), and downward flow (-1°, -30°, -80°, -90° from horizontal). Superficial gas and liquid velocities in m/sec are used as coordinates. Flow regimes vary significantly with inclination angle shown by the solid boundary curves drawn on the plots.

Risk function of the model, which is the summation of empirical risk (training error by comparing the model result with the actual values) and statistical confidence interval. A simple example shows how the separating hyperplane of SVM model separate different sets of data (see Figure 3.9) (Jahanbakhshi et al., 2012).

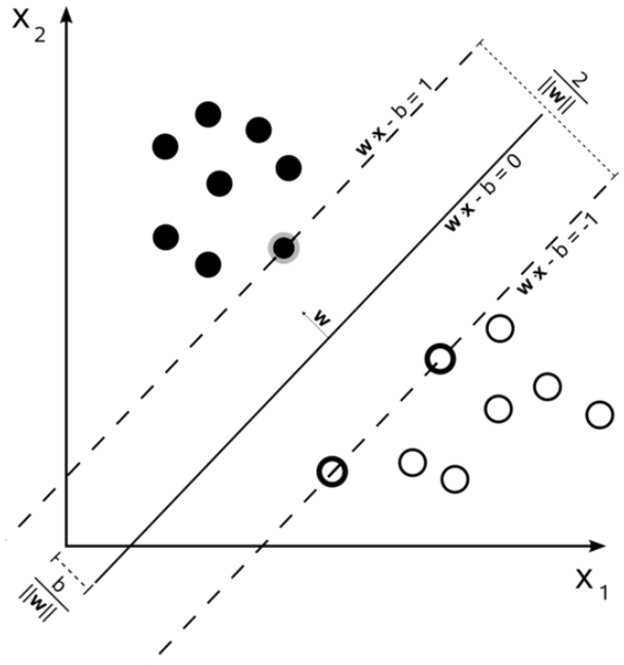

Figure 3.9: To classify these two different classes, black dots and circles, a Support Vector Machine model can find a separating hyperplane. SVM algorithm can ensure that the separating plane has maximal marginal distance to each class to find global optima. The outermost points of each class on the dashed lines are call support vectors, which is found by SVM models and used to classify new input data.

In the petroleum industry, some efforts have been made to apply SVM methods in various areas, such as oil and gas properties prediction and reservoir characterization. Nazari, Kuzma and Rector (2011) used the SVM method to predict permeability from well log data and core measurements and showed a good match and a high correlation coefficient in the training feature domain. El-Sebakhy et al. (2007) applied the SVM method for regression modeling to estimate oil formation volume factor based on four input variables, solution gas-oil ratio, reservoir temperature, oil gravity and gas relative density. The statistical analysis of prediction results showed that developed modeling scheme was superior to both standard

artificial feed-forward neural network and the most published empirical correlations. The SVM method can also be used to predict differential pipe sticking (Jahanbakhshi et al., 2012). Their results indicated that both SVM and conventional ANN methods could be of great use in different situations, however, the SVM approach was more applicable than ANN approach in differential pipe sticking prediction in both well planing stage and real-time drilling operations.

3.2.2 Model Training

This study adopted the gas and liquid velocity numbers by Duns and Ros (1963) as input variables to compare with the flow pattern maps by Mukherjee (1979) within the range of horizontal and upward flow. The velocity numbers implicitly include superficial phase velocity, liquid density, liquid-gas surface tension as shown in Equations 2.4 and 2.5. To consider the inclination angle effect on flow regime transition, the inclination angle from horizontal was also included into model input variables. The only output variable of the model is the predicted flow pattern. Four different flow patterns were considered to cover horizontal and upward flow, including bubble flow, slug flow, annular mist flow and stratified flow. The model structure is shown in Figure 3.10, where $\kappa(x_i, x_j)$ is called a kernel function, which can remove the non-linearity of the data.

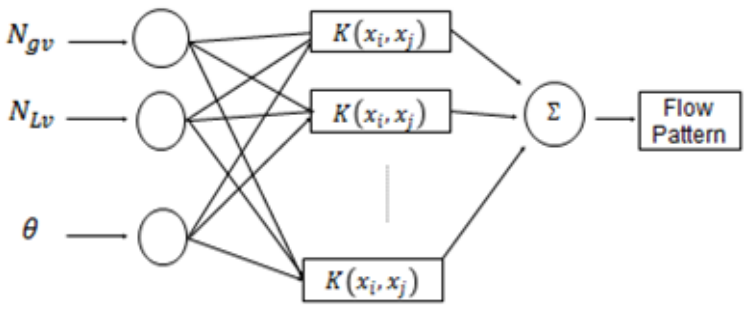

Figure 3.10: Flow pattern SVM model with a three-layer structure. Input layer consists of three input neurons, including gas velocity number, liquid velocity number and inclination. The middle layer contains kernel functions to transfer data to high dimension space, thus avoid non-linearity. The output layer outputs predicted flow pattern.

The data to train the SVM model comes from PhD thesis of Mukherjee (1979). All the experimental data with flow pattern observations were organized into one table of four columns, included in Appendix A, of which each row represents one data point of gas velocity number, liquid velocity number and inclination angle from horizontal. Fluids petrophysical properties were calculated from the recommended regression equations in Mukherjee's thesis to estimate gas and liquid velocity number. Since in actual field operations, downhill flow is not likely to happen, only upward and horizontal flow data were considered in this study for field application.

After flow pattern data at 45° and 60° inclination angles were removed due to sparsity, 598 measurements were left as seen in Figure 3.11 and Figure 3.12. The initial model training was not successful with the slug flow regime taking over most of the predicted flow map. This is because the portion of slug flow regime data points in the training data set was too large (379/598 data points = 63.4%) . Hence, some synthetic data for other flow regimes were added to the training data sets to maintain the balance of the data point numbers. In addition, a few data points on the original data plot were observed in the wrong flow regimes, probably due to experimental error These data points were also fixed in the final training data sets. The flow regime plots for the final data sets used to train the models are shown in Figure 3.13 and Figure 3.14.

Since there are some existing toolboxes for SVM models and algorithm design and implementation are time-consuming, this study uses a SVM library, LIBSVM, developed by Chang and Lin (2011). Even with these basics, to properly train the model and output better visualization, several hundreds lines of code was written in MATLAB. The kernel function used for model training is Radial Basis Function (RBF) by default, $\kappa(x_i, x_j) = e^{\left(-\gamma\|x_i - x_j\|^2\right)}, \gamma > 0$. The most difficult parameters for SVM model training is penalty parameter, c and kernel function parameter, γ, which cannot be predetermined but must be chosen by the users. To determine optimal values for these two parameters, a Grid Search optimization method was applied. Literally, Grid Searching is simply exhaustive searching for an optimal value

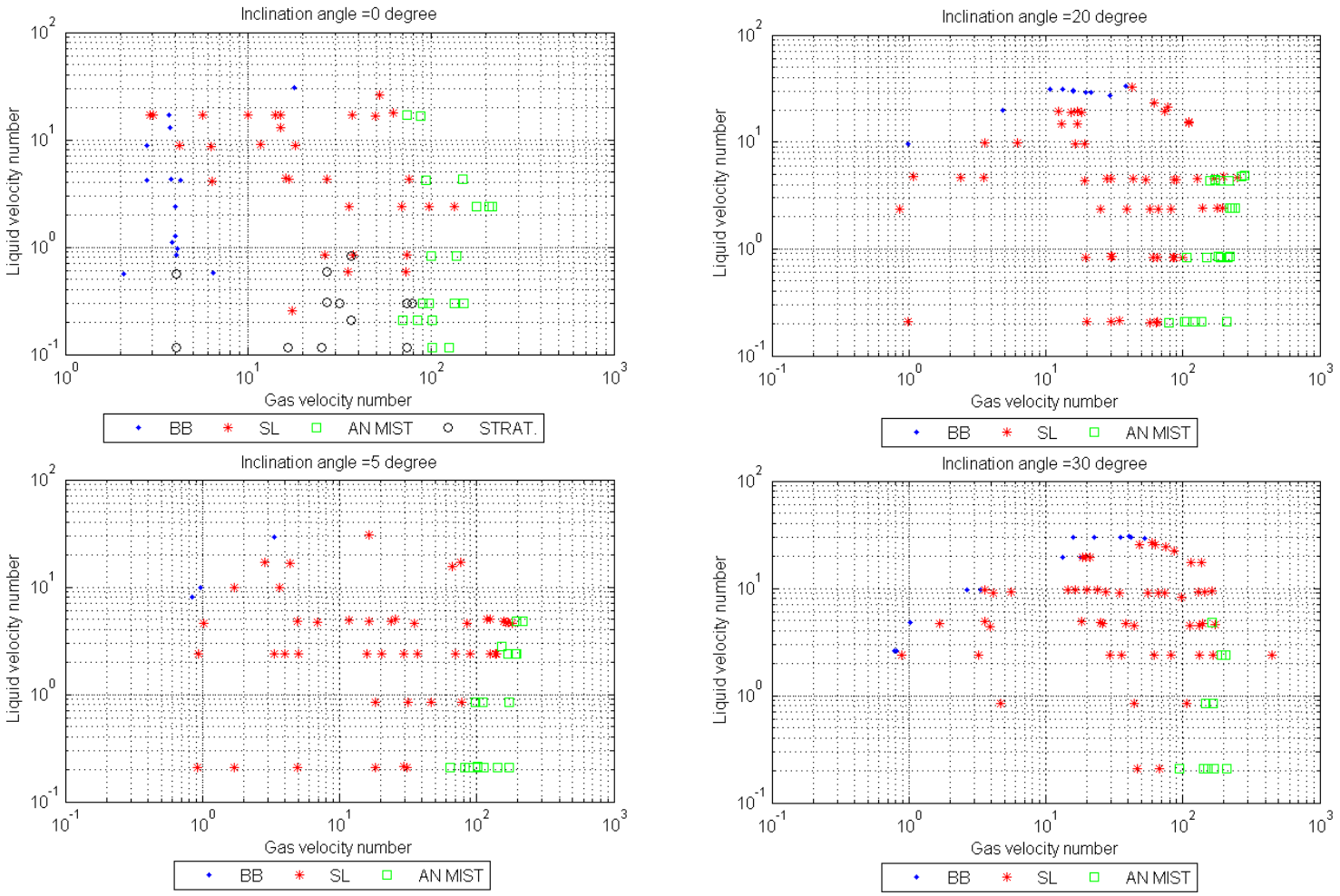

Figure 3.11: Original training data plot from Mukherjee (1979)'s thesis, Part 1. Note that the stratified flow pattern only exists near horizontal ($0^\circ \leq$ inclination angle $< 5^\circ$) and that as inclination angle increases, stratified flow pattern disappears and bubble flow and slug flow and annular mist flow are left. The geometries of flow regime transition boundaries change significantly on the flow pattern maps as horizontal flow transfers to upward flow. Noted that the inclination angle is the angle from horizontal direction on the maps.

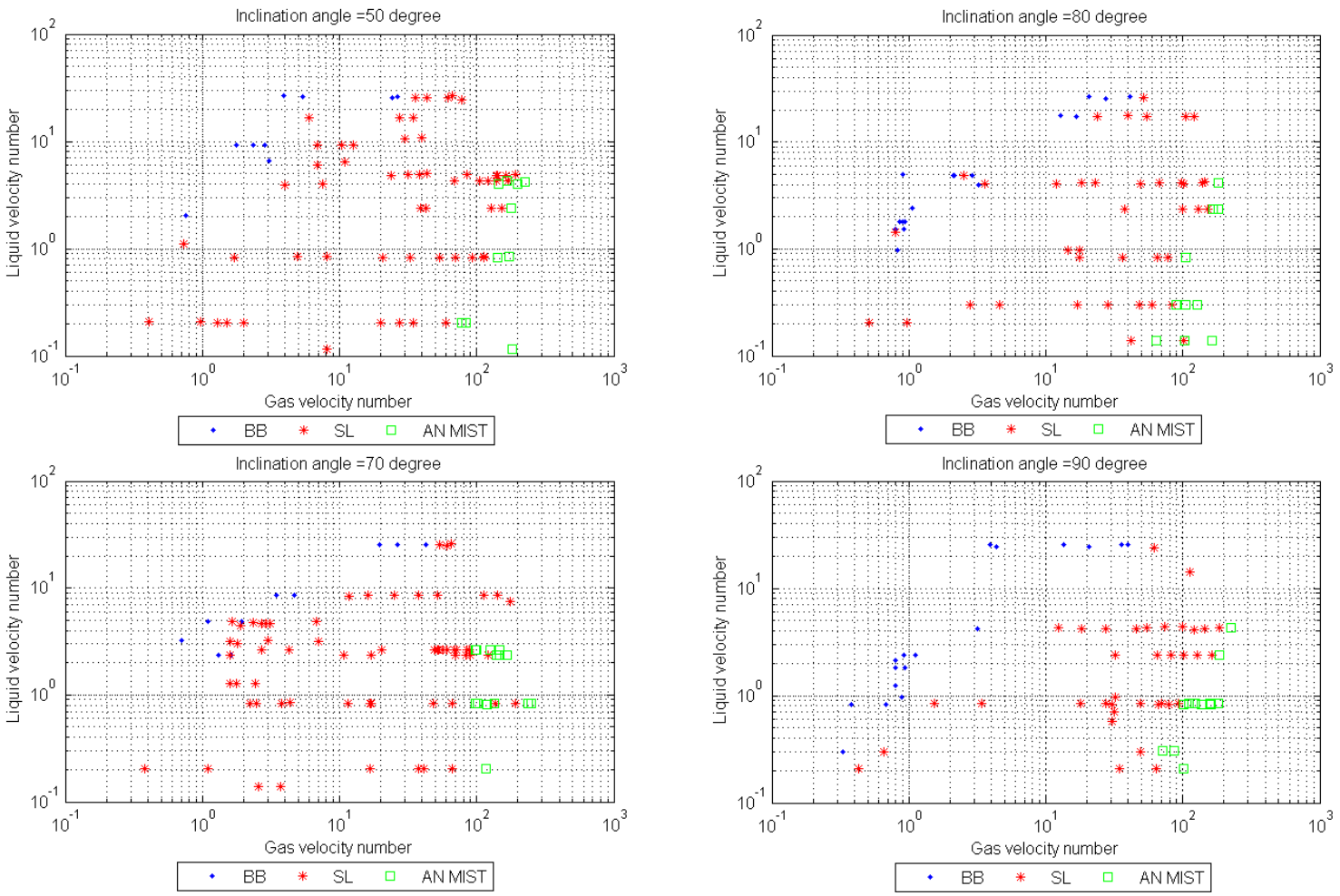

Figure 3.12: Original training data plot from Mukherjee (1979)'s thesis, Part 2. Combining with Part 1, we can see as inclination angle increases, the distribution of different flow regimes does not change significantly for upward flow. The boundary between bubble flow and slug flow is pushing towards slug flow and increasing bubble flow region, while the boundary between slug flow and annular mist flow stays in the area around gas velocity number of 100. These boundary behaviors show the similarities and differences the flow pattern maps can have at different inclination angles, if gas and liquid velocity numbers are chosen as coordinates. Noted that the inclination angle is the angle from horizontal direction on the maps.

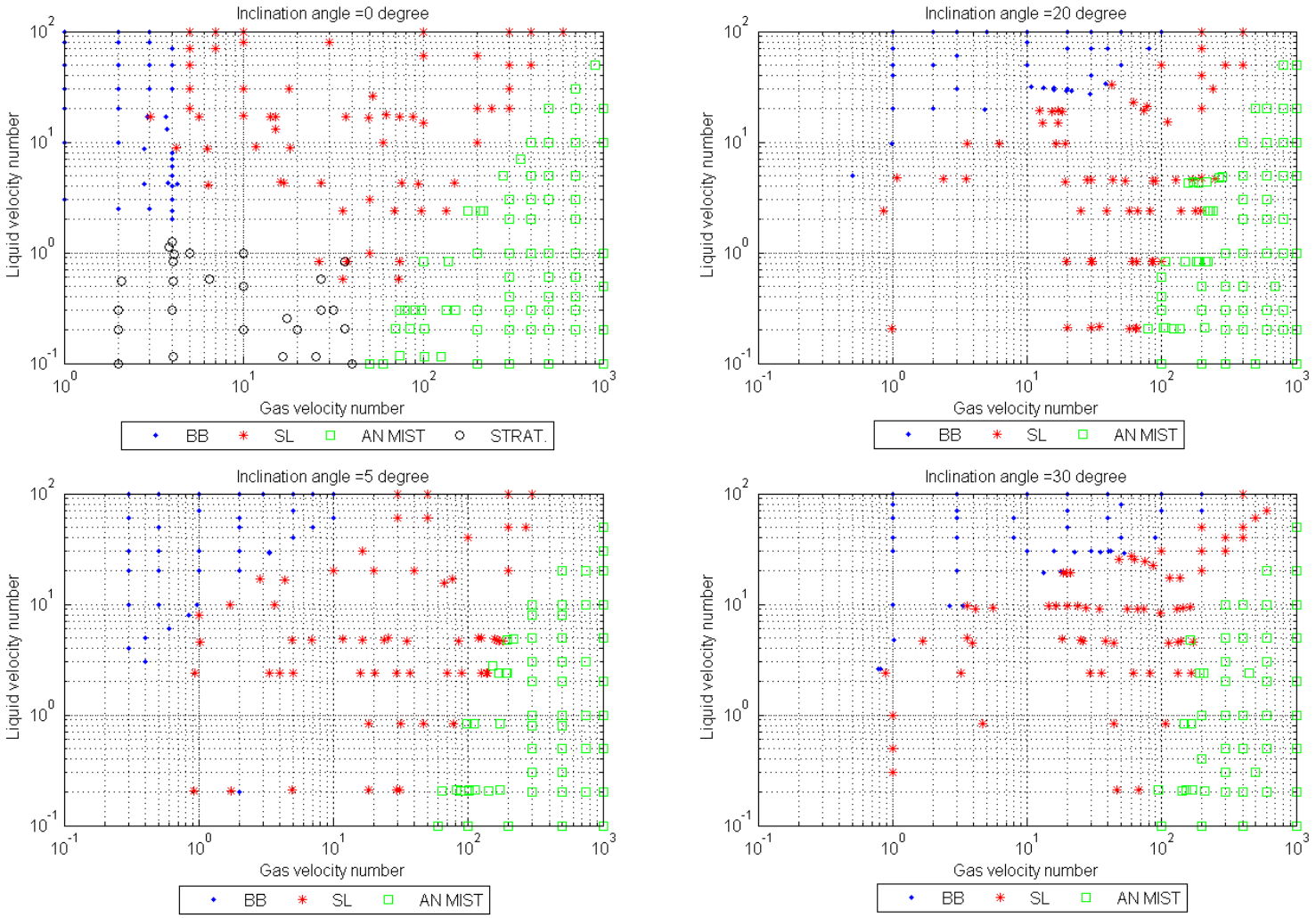

Figure 3.13: Modified training data plot based on Mukherjee (1979)'s thesis, Part 1. Noted that the inclination angle is the angle from horizontal direction on the maps.

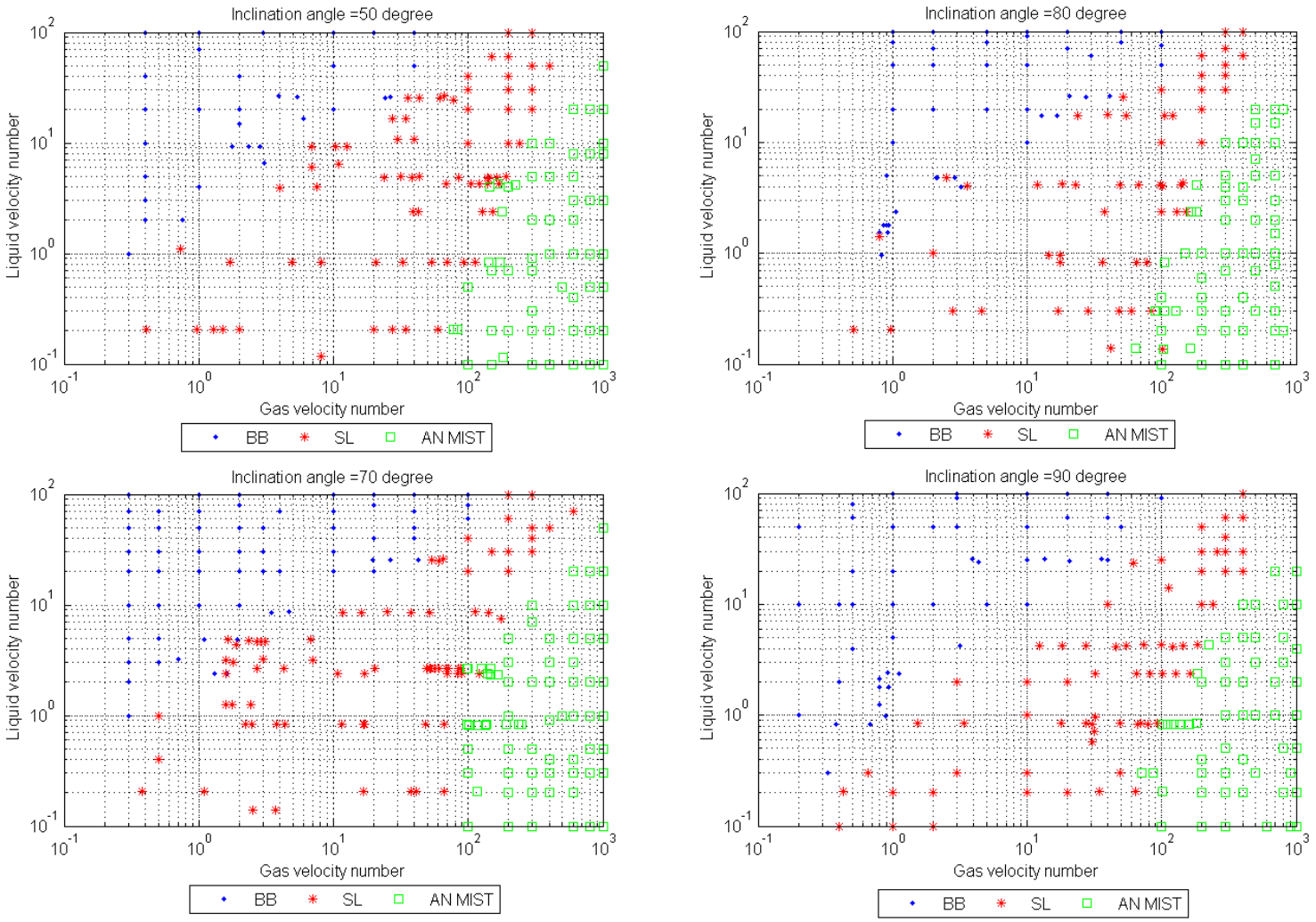

Figure 3.14: Modified training data plot based on Mukherjee (1979)'s thesis, Part 2. Due to the unsuccessful attempt of model training, some synthetic data were added into the training data set to maintain the balance between different flow regimes. As discussed in subsection of Flow Pattern Maps, the condition sets of each flow regime are believed to be continuous. Selection of additional data points obeys this rule. Comparisons between original data plots and modified data plots show that the synthetic data is selected only within each flow regime region or on the boundaries based on the original plots. Noted that the inclination angle is the angle from horizontal direction on the maps.

by comparing each grid value. For example, m number of values are selected for c within certain range and n number for γ. There will be $m \times n$ different combinations/grids for c and γ. The accuracy of the prediction model using different $c - \gamma$ combinations were plotted as a contour plot in Figure 3.15 and as a 3-D plot in Figure 3.16 to search where the optimal may locate.

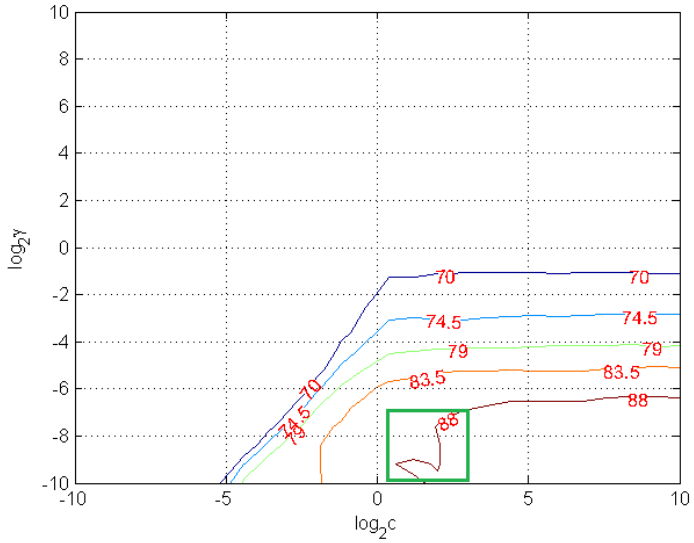

Figure 3.15: Contour plot of the prediction accuracy using the Grid Search method to search optimal $c - \gamma$ combination. The area where the optimal value is likely to exist is circled by a green box, since it associates with high accuracy and lower c value.

It should be noted that parameter c calculates the penalty for the training set error and that increasing the c value will increase the prediction accuracy for training set, but lose the generalization ability to predict other data sets, such as a test set, which can also be called "over-fitting". Hence, if there were multiple combinations for the highest accuracy, the one with lowest c value should be chosen. The search area is narrowed down to the green box in Figure 3.15 and finally, a combination of 3 and 0.003 were chose for c and γ, respectively, by comparing several different values in the green box.

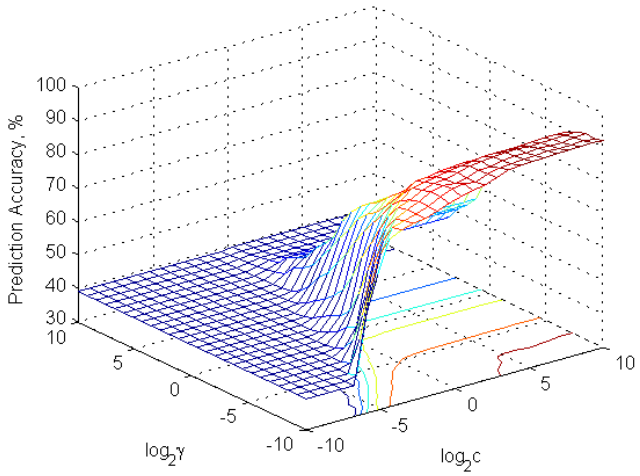

Figure 3.16: 3-D plot shows how prediction accuracy changes with $c - \gamma$ values, which confirms the contour plot in Figure 3.15.

3.2.3 Results

A SVM model for upward and horizontal flow was trained based on the data set described in Section 3.2.2 using the LIBSVM tool, with an accuracy of 93.0% (Chang and Lin, 2011). The prediction results are plotted in Figure 3.17, Figure 3.18 and Figure 3.19 for every ten degree from horizontal to vertical. To cover a wide variety of the field operating conditions, the prediction condition range of this model is, 0 to 90 for inclination angle, 0.1 to 1000 for gas velocity number and 0.01 to 100 for liquid velocity number. Moreover, some 3-D plots for all the possible flow patterns at all inclination angles within the studied condition range were generated and shown in Figure 3.20, Figure 3.21, Figure 3.22 and Figure 3.23. As seen in these figures, the model can provide a clear visualization of different flow patterns existing in different flow conditions with the inclination angle effect included.

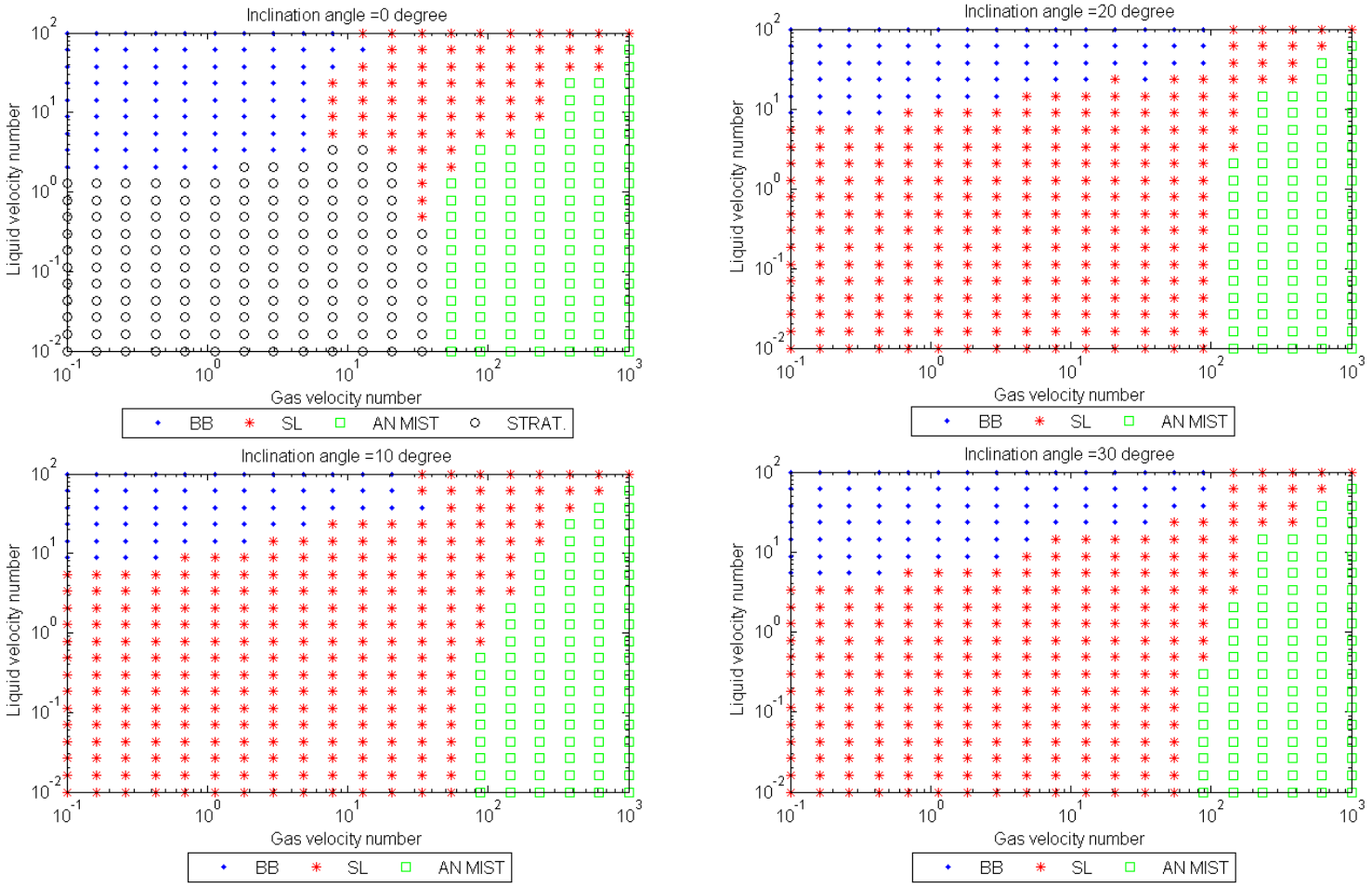

Figure 3.17: Prediction results, Part 1. The results show that the trained SVM model does recognize stratified flow pattern in horizontal flow and does not output stratified flow pattern as inclination angle increases. The transition boundaries are generated by model based on input training data and much clearer than those on the training data plots. Each flow regime exhibits in its own continuous area on the predicted flow pattern map. Slug flow region is in the middle and surrounded by bubble flow and annular mist flow in upward flow. Noted that the inclination angle is the angle from horizontal direction on the maps.

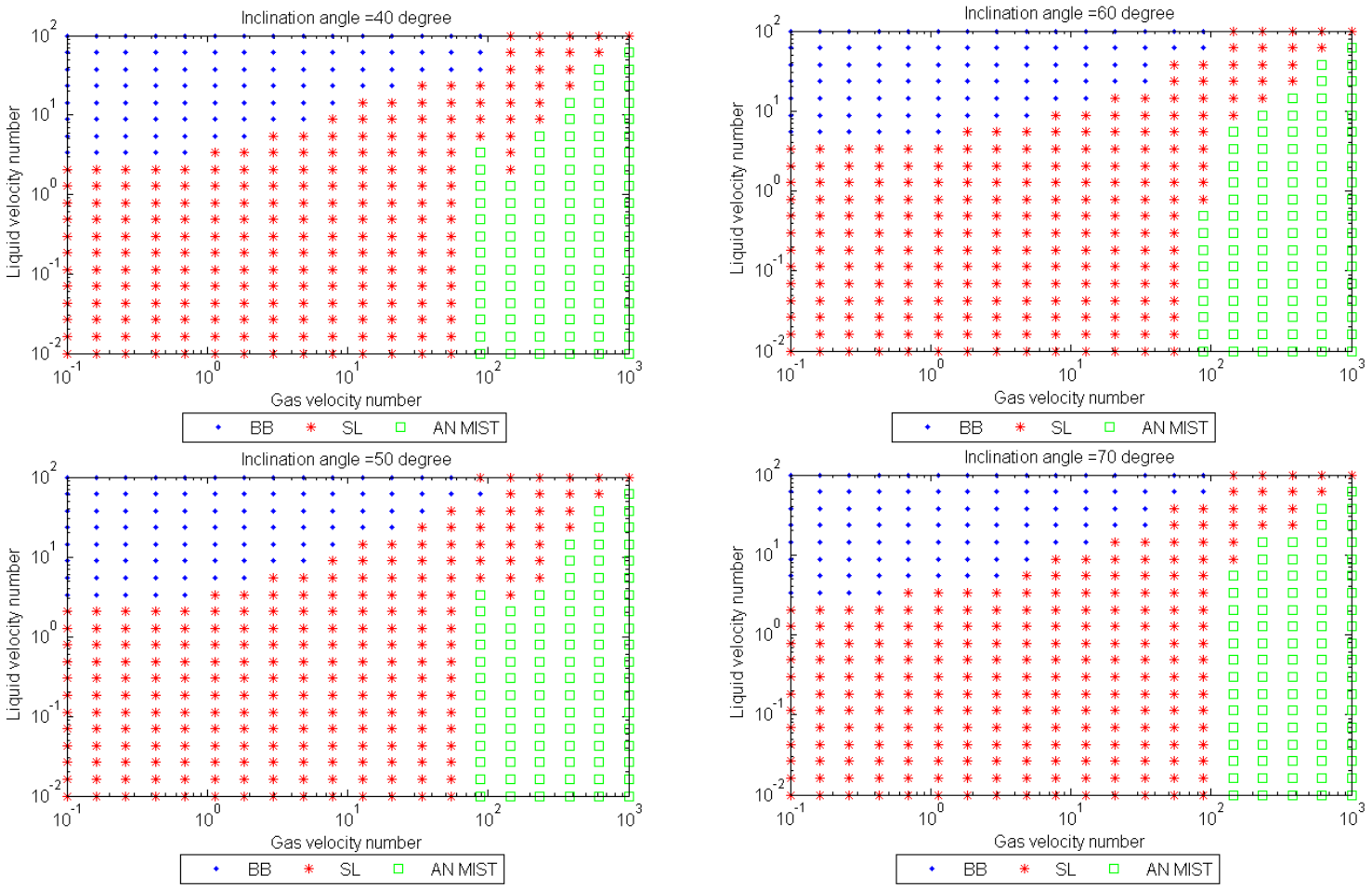

Figure 3.18: Prediction results, Part 2. The prediction result plots prove that the SVM model is more than a representation of the training data and that it has interpolation ability to predict flow pattern distribution for any angle between two given angles where training data is available. However, correlation equations do not possess this kind of property, thus may lose accuracy for the inclination angle where flow pattern data is not provided. Noted that the inclination angle is the angle from horizontal direction on the maps.

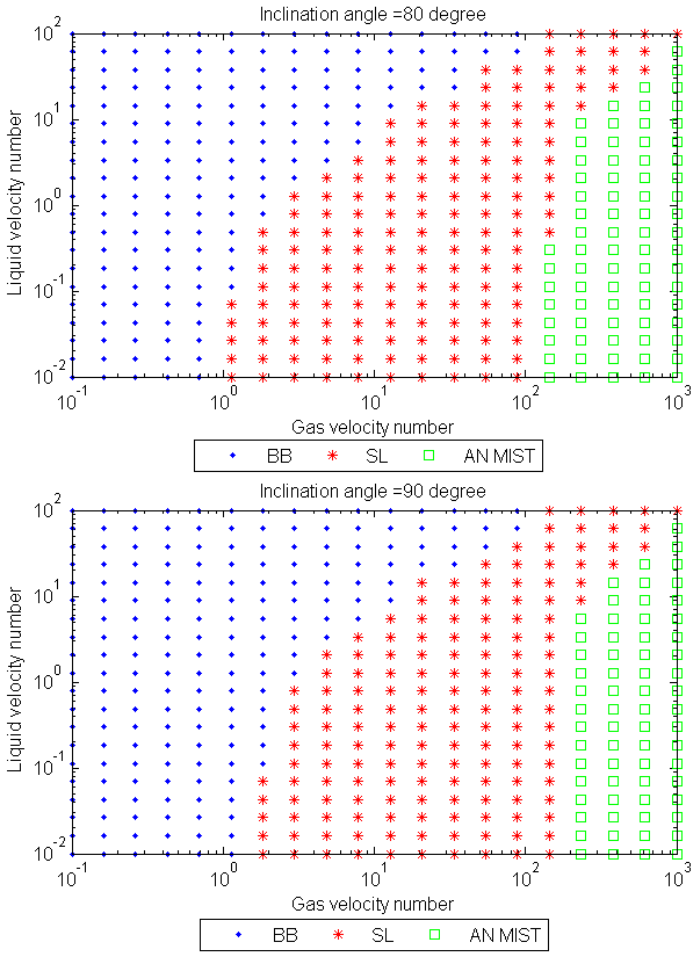

Figure 3.19: Prediction results, Part 3. Compare with the prediction results in Figure 3.20 and Figure 3.21 and we can see the model can capture the changes or features in training data that the bubble flow region is expanding and pressuring on the slug flow region in the middle and that the boundary between slug flow and annular mist flow remains around the area where gas velocity number is 100. In order to show the prediction performance for wider range, the axis range of liquid velocity number is increased as (0.01 to 100) wider than the data plot range of (0.1 to 100). Noted that the inclination angle is the angle from horizontal direction on the maps.

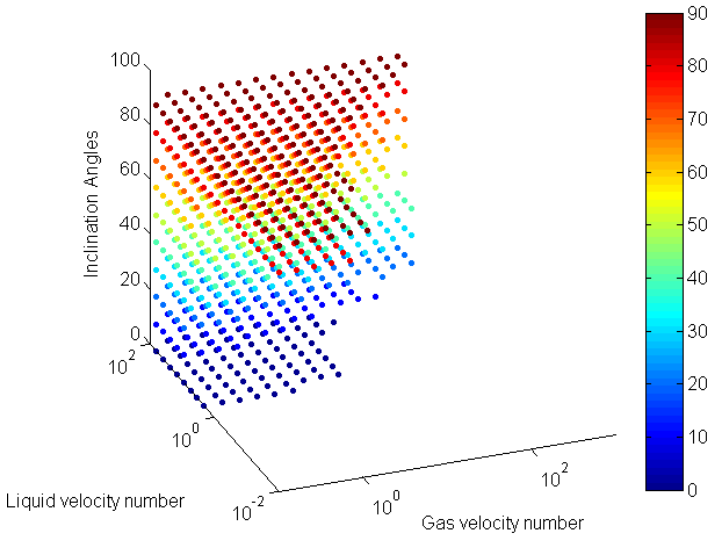

Figure 3.20: SVM model predicted bubble flow region in 3D plot provides a better visualization of the distribution of bubble flow pattern for inclination range of 0° to 90°. Note that the color map on the right indicates the magnitude of inclination angle. Noted that the inclination angle is the angle from horizontal direction on the maps.

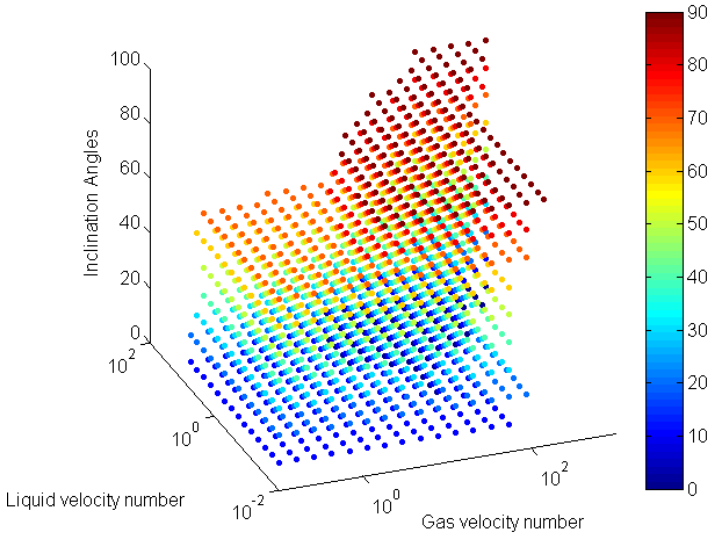

Figure 3.21: SVM model predicted slug flow region in the middle of the 3D plot and surrounded by bubble flow and annular mist flow. Noted that the inclination angle is the angle from horizontal direction on the maps.

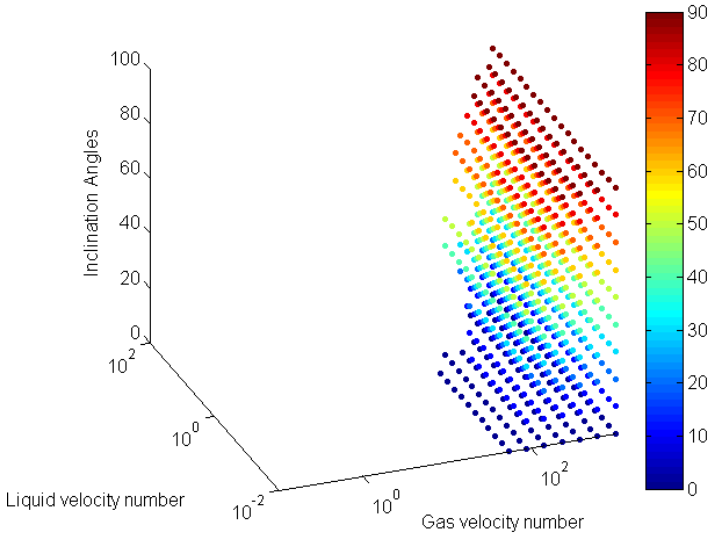

Figure 3.22: SVM model predicted annular mist flow pattern appears as gas and liquid velocity numbers increase. Noted that the inclination angle is the angle from horizontal direction on the maps.

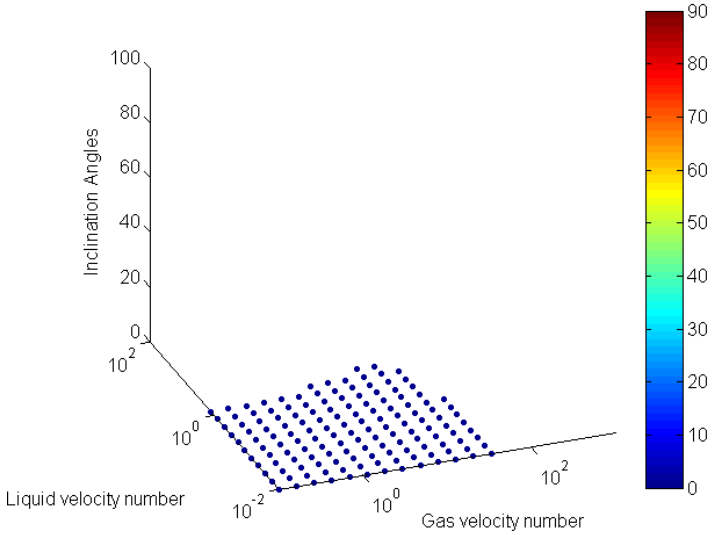

Figure 3.23: SVM model predicted stratified flow region only exists near horizontal and disappears for upward flow. Noted that the inclination angle is the angle from horizontal direction on the maps.

CHAPTER 4

MULTIPHASE FLOW PRESSURE DROP CALCULATION

The total pressure gradient for fluid flow in pipes can be expressed in three parts, the elevation pressure gradient, the friction pressure gradient, and the acceleration pressure gradient as shown in Equation 4.1 (Brill and Mukherjee, 1999).

$$\left(\frac{dP}{dL}\right)_t = \left(\frac{dP}{dL}\right)_{el} + \left(\frac{dP}{dL}\right)_f + \left(\frac{dP}{dL}\right)_{acc} \tag{4.1}$$

where, $\left(\frac{dP}{dL}\right)_t$ = total pressure drop, $psia/ft$;
$\left(\frac{dP}{dL}\right)_{el}$ = elevational pressure drop, $psia/ft$;
$\left(\frac{dP}{dL}\right)_f$ = frictional pressure drop, $psia/ft$; and,
$\left(\frac{dP}{dL}\right)_{acc}$ = accelerational pressure drop, $psia/ft$.

The first term comes from the gravity effect on the fluids in flow, often called the hydrostatic head. The elevational component is normally predominant in the total pressure gradient and easier to calculate by multiplication of mixture density, gravitational conversion constant and the sine of the inclination angle from horizontal. Frictional pressure loss results from the frictions or shear stresses at the pipe wall or those acting between different phases. Accelerational pressure drop due to kinetic energy change is normally neglected except under the conditions of high mass flow rates and low tubing pressures. Work by Hagedorn and Brown (1965) indicated that under these conditions, the pressure losses as a result of the acceleration gradient may constitute as much as ten percent of the total pressure drop near the top of well.

In multiphase flow pressure drop calculations, liquid holdup and friction factor calculations mainly correspond to elevational pressure gradient and frictional pressure gradient, respectively, while the flow pattern significantly affects the physical mechanism of flow and thus the way these two terms are handled.

4.1 Bottom-hole Pressure Calculation Procedure

In field operations, knowing the bottom-hole pressure (BHP) is of importance. However, in most cases, a direct measurement by a downhole gauge is not always economic, practical or feasible. Under these circumstances, the bottom-hole pressure is usually calculated from the pressure data measured at surface and estimating the pressure gradient along the well. Because the pressure gradient changes along the entire well, it is unrealistic to calculate an average pressure gradient and multiply it by the well length to get an adequate answer, therefore a well length is usually broken down into segments and one pressure gradient calculation will be performed on each segment. This piece-wise calculation will then proceed from the wellhead to the bottom of the wellbore to get the final BHP value, see Figure 4.1.

4.1.1 Fluid Property Correlation

To perform pressure gradient calculations on each segment, fluids properties first have to be estimated. Table 4.1 lists all of the petrophysical correlations for fluids properties calculation used in this study. If there is more than one correlation for a property, the first correlation is set as the default.

4.1.2 Bottom-hole Pressure Calculation Flow Chart

A multiphase flow bottom-hole pressure calculator was written in FORTRAN to implement the existing multiphase correlations and built ANN models for this research. This calculator will be described later in Section 5.2. The process of how the bottom-hole pressure calculation is performed is shown in Figure 4.1. This study incorporates the piece-wise calculation from wellhead to bottom-hole. First, required input data is introduced to the calculator and an initialization of calculation variables at the wellhead takes place. The fixed pressure drop method is adopted, which requires fixing a pressure drop on each well segment and then calculating the length of segment to correspond to this much pressure drop. The pressure drop $\triangle P$ is fixed to be the smaller of 100 psi and one tenth of the last calculated pressure or the initial pressure P_0. The well segment length $\triangle MD$ calculation is an iteration

process.

Table 4.1: Petrophysical Correlations List

Fluids Properties	Correlation
Oil Viscosity, < PB (Bubble Point)	Beggs and Robinson (1975)
Oil Viscosity, > PB	Vazquez and Beggs (1980)
Water Viscosity	Van Wingen (1950)
Liquid Mixture Viscosity	The same with continuous phase (Inversion Water Volume Fraction: Brinkman (1952))
Gas-Oil Surface Tension	Abdul-Majeed and Abu Al-Soof (2000); Baker and Swerdloff (1956)
Gas-Water Surface Tension	Sutton (2009); Hough, Rzasa and Wood (1951)
Solution Gas/Oil Ratio and PB	Vazquez and Beggs (1980); Lasater (1958); Standing (1947)
Solution Gas/Water Ratio	Culberson and McKetta (1951)
Dissolved Gas Specific Gravity	Katz (1942)
Free Gas Gravity	Material Balance
Oil Formation Volume Factor, < PB	Vazquez and Beggs (1980); Standing (1947)
Oil Compressibility & Formation Volume Factor, > PB	Vazquez and Beggs (1980)
Water Formation Volume Factor	Gould (1974)
Water Density	Rowe and Chou (1970)
Gas Density	Real Gas Law
Gas Viscosity	Lee, Gonzalez and Eakin (1966)
Gas Pseudocritical Pressure and Temperature	Sutton (2007); Hall and Yarborough (1973)
Darcy-Weisbach Friction Factor	Colebrook and White (1937)
Gas Compressibility Factor	Dranchuk and Kassem (1975); Hall and Yarborough (1974); Brill and Beggs (1979); Standing (1981)

First an assumed segment length $\triangle MD_0$ is set; then $\triangle P$ and $\triangle MD_0$ are used to calculate average pressure, average temperature and some intermediate variables as shown in Figure 4.1. For the first segment at the wellhead, $\triangle MD_0$ is set to be one-tenth of plug-back total depth; for the rest, it is the last calculated segment length. With the help of multi-

phase correlations or ANN models, the total pressure gradient $\left(\frac{dP}{dL}\right)_t$ on this segment can be calculated. So the segment length will be a fixed pressure drop divided by the total pressure gradient. The calculated segment length $\triangle MD$ is then compared with the assumed one $\triangle MD_0$. If the difference is within one foot, the calculation proceeds to the next segment. Otherwise, the average of assumed and calculated segment lengths are set to be the new assumed one and the process iterates until the difference is less than one foot. The calculation moves on one piece by one piece, until the measured depth reaches bottom-hole. The final results and variables on each segment are then printed to an output file by calculator.

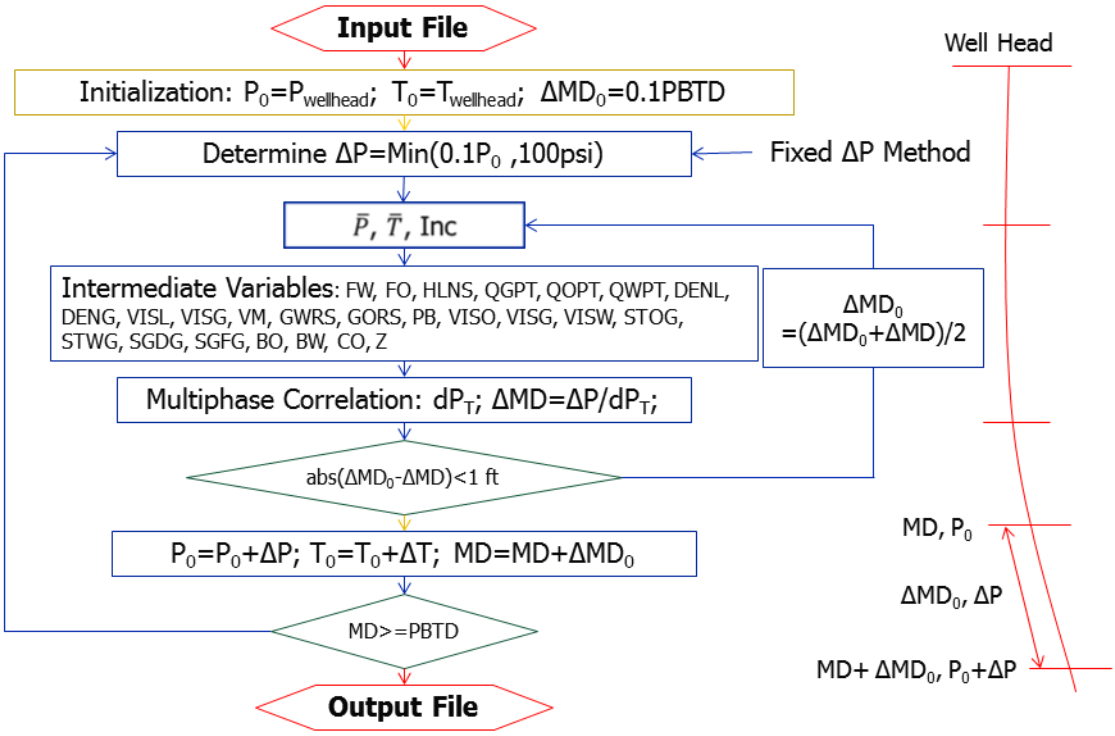

Figure 4.1: Bottom-hole pressure calculation flow chart. The piece-wise calculation moves from wellhead to bottom-hole. On each well segment, the pressure drop is first fixed and the corresponding well segment length is then solved using multiphase correlations or ANN models. Two files, an input file and an output file are generated for each BHP calculation.

4.2 Artificial Neural Network (ANN) Approaches

To discover the possibilities for improving BHP prediction, we can review previous work including multiphase correlations and ANN approaches and also examine their calculation procedures.

As described in Section 2.2.2, the studies done by Ternyik et al. (1995), Osman, Ayoub and Aggour (2005), Ozbayoglu and Ozbayoglu (2007), Mohammadpoor et al. (2010), Ashena et al. (2010), and Al-Shammari (2011), have some similarities. No matter what type of ANN or what ANN structure they used, the bottom-hole pressure was directly set to be the output of the model. Thus there is only a one-time estimation performed on the entire length of well. Even though ANN models outperform multiphase correlations in many cases, high accuracy prediction only occurs when the test data comes from the same source with training data. No flow pattern is considered or involved in ANN model calculations.

Reviewing the procedures for multiphase correlations, these calculations are piece-wise and never done by only one estimation. Before each pressure gradient estimation, the flow pattern is predicted and a corresponding set of pressure loss equations or correlations is then chosen and ready for the pressure gradient calculation.

By comparing these two methods above, we can note two differences:

- ANN approaches lack piece-wise calculations and just use some variables measured at the wellhead as input variables and bottom-hole pressure as the output variable and consequently model the multiphase flow pressure changes for the entire well length;

- ANN approaches do not adopt the way multiphase correlations calculate BHP in that the flow pattern is first predicted and the corresponding pressure gradient correlation is then chosen to estimate the total pressure drop.

Which one should we choose or which one is more accurate and has a wider prediction range? First, piece-wise calculation is like a finite-different method and a one-time estimation is like the average value between the wellhead and bottom-hole. Thus, piece-wise calculation

should have a stronger ability to handle complex problems versus a one-time estimation. Second, as discussed in Chapter 3, the flow pattern is one of the key factors that can affect the pressure drop mechanism significantly. Thus, to have flow patterns considered such as the multiphase correlation does should be the proper way to handle the pressure calculation. Third, many papers suggest that the prediction performance of ANN model is superior to multiphase correlations or mechanistic models (Al-Shammari, 2011; Ashena et al., 2010; Mohammadpoor et al., 2010; Osman, Ayoub and Aggour, 2005; Ozbayoglu and Ozbayoglu, 2007; Ternyik et al., 1995). The conclusion from these points in that it is acceptable to implement ANN models into multiphase correlation calculation procedures.

4.2.1 Back-propagation Neural Network Implementation

Based on the review of multiphase correlation calculation procedures, some BP (back-propagation) neural network models can be used to replace correlations to estimate pressure loss. The calculation procedure structure remains unchanged in that each segment's flow pattern is determined first and that instead of correlations, some BP NN (neural network) models are used to predict the pressure gradient. In order to accomplish this implementation, there should be at least as many neural network models as possible flow patterns, i.e., as least four models are needed to cover bubble flow, slug flow, annular mist flow and stratified flow.

4.2.2 Back-propagation Neural Network

Based on the above discussion, some specifications for suitable neural network models, such as the short-length calculation on well segment and input variables selection, limit the sources of data that can be collected to train models. Fortunately, the data measured on a 32 ft long test section from Mukherjee (1979) meets all the specifications, see Table 4.2. The inlet and outlet pressure gauges are 30.5 ft apart. The total data is divided into four parts based on the flow pattern observed and used to train pressure gradient prediction BP NN models. Ten variables believed to affect the pressure gradient are collected, including

inclination angle, liquid superficial velocity, gas superficial velocity, gas-liquid surface tension, liquid density, specific gravity of free gas, liquid viscosity, gas viscosity, average pressure, and average temperature. The only output variable is pressure gradient.

Table 4.2: BP Neural Network Model Training Data Description (Mukherjee, 1979)

Flow Regime	Number of Data	Data Range
Bubble Flow	86	kerosene-air; $\theta: 0 \sim 90°$; $\rho_L: 49.24 \sim 51.07\, lbm/scf$; $\bar{P}: 28.2 \sim 83.7\, psia; \bar{T}: 63 \sim 126\, F$;
Slug Flow	262	kerosene-air; $\theta: 0 \sim 90°$; $\rho_L: 48.10 \sim 51.64\, lbm/scf$; $\bar{P}: 25.4 \sim 91.9\, psia; \bar{T}: 43 \sim 165.5\, F$;
Annular Mist Flow	94	kerosene-air; $\theta: 0 \sim 90°$; $\rho_L: 49.27 \sim 51.72\, lbm/scf$; $\bar{P}: 25.9 \sim 90.7\, psia; \bar{T}: 40 \sim 125\, F$;
Stratified Flow	6	kerosene-air; $\theta: 0°$; $\rho_L: 49.59 \sim 50.90\, lbm/scf$; $\bar{P}: 28.2 \sim 70.9\, psia; \bar{T}: 68.5 \sim 114\, F$;

However, initial attempts in this research to train neural network models failed due the narrow conditioning range from this data source. To broaden the condition range of training data, the intermediate results from piece-wise calculations using multiphase correlations appeared to be a qualified candidate, since the results contain all the variable values calculated on each well segment instead of the entire length.

As discussed, there are eleven multiphase correlations considered in this study. The selection of which correlation's piece-wise calculation results to use depends on the correlation prediction accuracy to ensure data validity and accuracy. First, data with BHP measurements was collected from literature or fields, and is shown in Table 4.3. Then the BHP is calculated using the eleven multiphase correlations, and compared with actual pressure to determine which correlation has the highest prediction accuracy for each data point. Last, the segment calculation results from the determined correlation are used as training data sets to neural network models. Since piece-wise calculation requires the prediction of a flow regime before the pressure drop is estimated on each segment, the collected segment-scale

data sets are grouped based on the predicted flow regime. Because each well is broken down into multiple segments, one BHP sample will produce multiple neural network model training data sets. To ensure the validity and quality of the input data, the data sets that none of the correlations give an accurate prediction within 10% error are removed. Finally, 2196 data sets were collected from multiphase correlation calculation results for use in this research, and are shown in Table 4.4.

Table 4.3: Collected Bottom-hole Pressure Data

Data Source	Number of Data	Data Range
Eaton (1966)	263	two-inch and four-inch pipeline; water/crude/distillate and natural gas; $\theta: 0°$; $\rho_L: 48.05 \sim 63.02\, lbm/scf$; $\bar{P}: 70 \sim 950\, psig$;$\bar{T}: 65 \sim 117\, F$; $\mu_L: 1 \sim 13.5\, cp$
Peffer, Miller and Hill (1988)	94	water-oil-gas; $\theta: 90°$; $\rho_L: 34.44 \sim 58.09\, lbm/scf$; $\bar{P}: 551.5 \sim 3632\, psia$;$\bar{T}: 79 \sim 213.5\, F$;
Asheim (1986)	37	oil-gas; $\theta: 43.7 \sim 90°$; $\rho_L: 52.54 \sim 52.85\, lbm/scf$; $\bar{P}: 1079.2 \sim 1476.2\, psia$;$\bar{T}: 188.5 \sim 194\, F$;

Table 4.4: BP Neural Network Model Training Data Description - from Multiphase Correlation Calculation Results

Flow Regime	Number of Data	Data Range
Bubble Flow	109	horizontal flow data:θ : 0°; v_{sL} : $0.7936 \sim 0.7954\, ft/sec$; v_{sg} : $0.2947 \sim 0.3003\, ft/sec$; σ_L : $18.20 \sim 18.23\, dynes/cm$; ρ_L : $45.84 \sim 45.96\, lbm/ft^3$; SG_g : 0.56; μ_L : $1.303 \sim 1.357\, cp$; μ_g : $0.01207 \sim 0.01212\, cp$; $\bar{P}$: $333.0 \sim 333.4\, psia$;$\bar{T}$: $92.36 \sim 94.86\, F$; upward flow data: θ : $43.7 \sim 90$°; v_{sL} : $0.0568 \sim 10.85\, ft/sec$; v_{sg} : $0.000659 \sim 2.0\, ft/sec$; σ_L : $5.35 \sim 10.79\, dynes/cm$; ρ_L : $46.45 \sim 48.53\, lbm/ft^3$; SG_g : $1.1 \sim 1.122$; μ_L : $0.479 \sim 1.358\, cp$; μ_g : $0.0140 \sim 0.0186\, cp$; $\bar{P}$: $955.9 \sim 1688.9\, psia$;$\bar{T}$: $167.68 \sim 235.71\, F$;
Slug Flow	1225	horizontal flow data:θ : 0°; v_{sL} : $0.1477 \sim 7.4144\, ft/sec$; v_{sg} : $0.5741 \sim 74.095\, ft/sec$; σ_L : $9.8337 \sim 68.2098\, dynes/cm$; ρ_L : $45.13 \sim 62.40\, lbm/ft^3$; SG_g : $0.56 \sim 0.6111$; μ_L : $0.0695 \sim 13.065\, cp$; μ_g : $0.0116 \sim 0.0130\, cp$; $\bar{P}$: $322.8 \sim 991.8\, psia$;$\bar{T}$: $71.48 \sim 117\, F$; upward flow data: θ : $43.7 \sim 90$°; v_{sL} : $0.0501 \sim 10.4545\, ft/sec$; v_{sg} : $0.0096 \sim 50.235\, ft/sec$; σ_L : $0.8691 \sim 25.1633\, dynes/cm$; ρ_L : $28.88 \sim 51.61\, lbm/ft^3$; SG_g : $0.56 \sim 1.122$; μ_L : $0.0726 \sim 6.557\, cp$; μ_g : $0.0100 \sim 0.0273\, cp$; $\bar{P}$: $158.2 \sim 4607.6\, psia$;$\bar{T}$: $74.76 \sim 243.94\, F$;

Table 4.4: Continued.

Flow Regime	Number of Data	Data Range
Annular Mist Flow	805	horizontal flow data:θ : 0°; v_{sL} : $0.0372 \sim 6.541\, ft/sec$; v_{sg} : $7.921 \sim 80.423\, ft/sec$; σ_L : $11.08 \sim 68.28\, dynes/cm$; ρ_L : $45.56 \sim 62.46\, lbm/ft^3$; SG_g : $0.573 \sim 0.6111$; μ_L : $0.748 \sim 18.641\, cp$; μ_g : $0.0115 \sim 0.01257\, cp$; $\bar{P}$: $323.04 \sim 880.89\, psia$;$\bar{T}$: $64.99 \sim 105.47\, F$; upward flow data: θ : 90°; v_{sL} : $0.01569 \sim 4.5032\, ft/sec$; v_{sg} : $4.616 \sim 53.566 ft/sec$; σ_L : $0.381 \sim 18.09\, dynes/cm$; ρ_L : $23.76 \sim 50.11\, lbm/ft^3$; SG_g : $0.56 \sim 0.785$; μ_L : $0.046 \sim 6.037\, cp$; μ_g : $0.0111 \sim 0.0229 cp$; $\bar{P}$: $472.5 \sim 4086.1\, psia$;$\bar{T}$: $59.87 \sim 272.40\, F$;
Stratified Flow	57	horizontal flow data:θ : 0°; v_{sL} : $0.0360 \sim 0.751\, ft/sec$; v_{sg} : $0.2919 \sim 9.689\, ft/sec$; σ_L : $17.96 \sim 68.58\, dynes/cm$; ρ_L : $45.09 \sim 62.35\, lbm/ft^3$; SG_g : $0.56 \sim 0.6111$; μ_L : $0.667 \sim 13.045\, cp$; μ_g : $0.0115 \sim 0.0124\, cp$; $\bar{P}$: $305.02 \sim 355.09\, psia$;$\bar{T}$: $72.44 \sim 112.06\, F$;

According to the input and output variables, the numbers of neurons on the input and output layers of the model are ten and one, respectively. This study adopts a three-layer structure, i.e. only one hidden layer. There is no exact guideline to follow to determine the optimum number of neurons on the hidden layer, except by trial and error. Different neural network model structures with changing neuron numbers on hidden layer were tested and compared to find a suitable hidden-layer neuron number. To increase the prediction accuracy of each neural network model, an optimization method, Genetic Algorithms (Mitchell, 2002),

was introduced to the training process. A Genetic Algorithm (GA) was inspired by the mechanism of genetic inheritance and the process of natural evolution. There are three basic operations in a GA optimization process, including selection, crossover, and mutation. In this study, the initial values for the weights and thresholds of neural network models are treated as one individual, then are optimized through repetitive application of the three basic operators, selection, crossover and mutation, until a least error is achieved. Since the collected data for bubble flow and stratified flow is insufficient for model training, only two BP neural network models are prepared for slug flow and annular mist flow. It should be noted that for a gas production well, slug flow and mist flow are more common than other two-phase flow patterns. A suitable hidden-layer number should not only ensure low prediction errors, but also should not be too large. Small hidden-layer numbers make the model structure too simple to handle complex problems. Although larger hidden-layer numbers appear to increase prediction accuracy, too large of a number can cause over-fitting problems. To avoid over-fitting and also ensure the model complexity, the hidden-layer neuron number ranges from 5 to 30 in this research. Figure 4.2 and Figure 4.3 show the relationships between total prediction errors of models with hidden-layer numbers. The hidden-layer numbers for slug flow and mist flow are set to be 30 and 28, respectively. This choice is somehow reasonable as slug flow has more complicated mechanisms than mist flow thus requiring a more complex structure.

4.3 Combined Bottom-hole Pressure Calculation Procedure

As discussed, accuracy and applicability are the two major concerns for pressure drop prediction. Artificial neural network techniques have been proven to outperform multiphase correlations in some aspects. However, the neural network models are restricted by the conditioning range of input training data. Hence, the idea of combining both multiphase correlations and ANN models aims to take both accuracy and applicability into account. As illustrated in Figure 4.4, once enough input data is gathered, the piece-wise calculation begins. On each well segment, the flow regime is first determined via either support vector

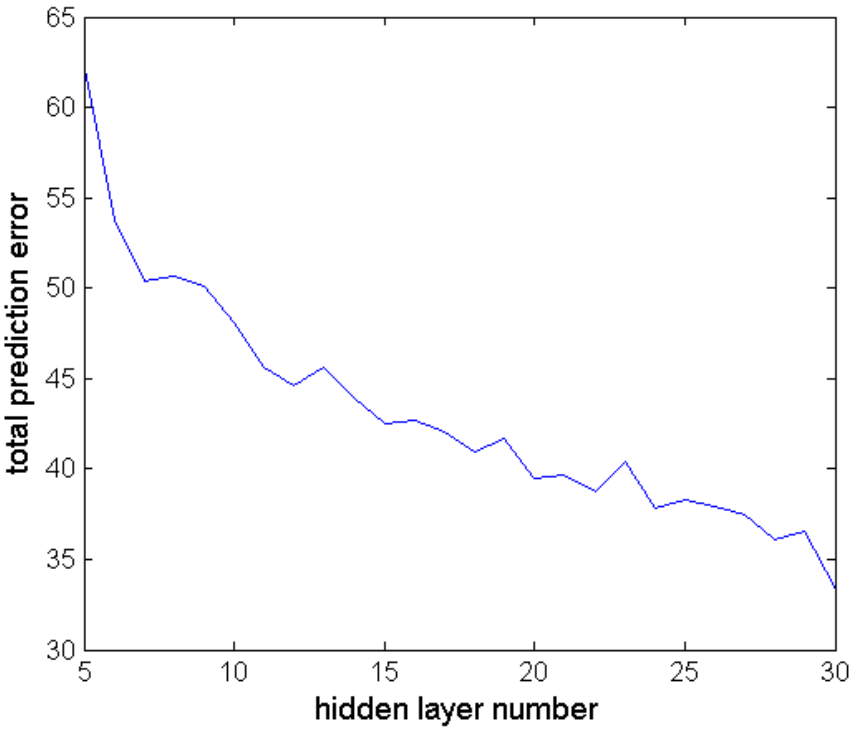

Figure 4.2: For the slug flow neural network model, the total prediction error drops as the hidden-layer number increases. Since the stepping down trend is continuous but getting flat and arbitrarily increasing neuron number to lower training error can cause over-fitting problem, the neuron number on the hidden layer is set to be 30, the upper range in this research. Hence, the model structure becomes, 10-30-1.

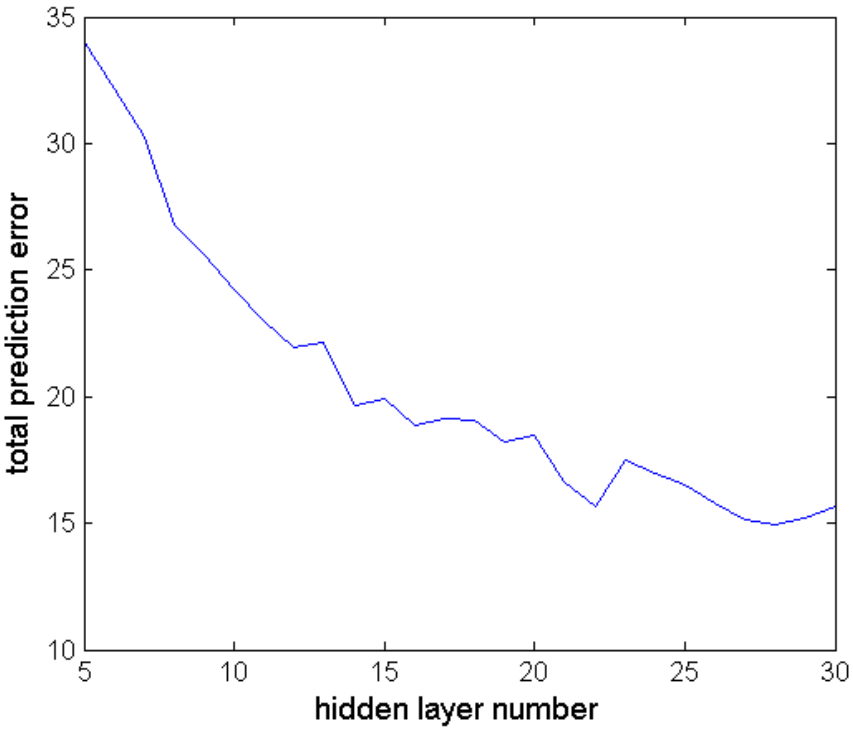

Figure 4.3: The prediction error decreases as the hidden-layer neuron number increases for the mist flow model. It can be seen that after total prediction error drops down at hidden-layer number of 28, the curve starts to go up a little bit. To avoid over-fitting and maintain a lower error, the hidden-layer number is selected as 28. Hence, a structure of 10-28-1 is used for mist flow model.

machine models or flow regime criteria of correlations and the pressure gradient then is estimated by either BP neural network models or multiphase correlations based on the condition range of input data. The process iterates until the difference between the assumed well segment length and calculated result is within tolerance. After one well segment calculation is finished, the calculation proceeds to the next one until the total length reaches bottom-hole.

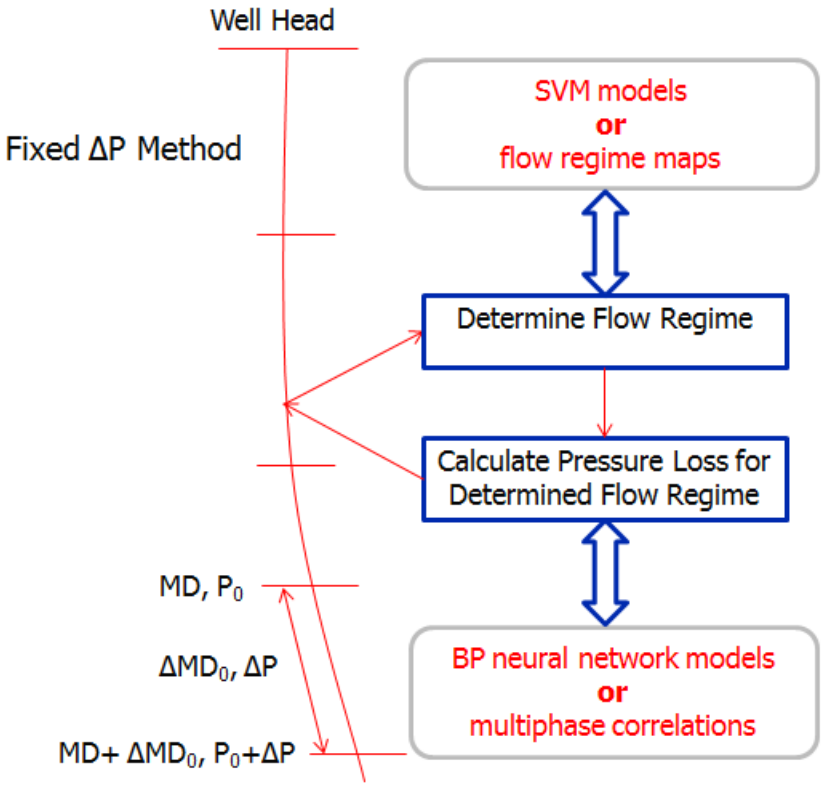

Figure 4.4: The flow chart of the combined bottom-hole pressure calculation procedure introduces artificial neural network models into the piece-wise calculation of multiphase correlations. Support vector machine models and flow regime maps can be used to predict the flow regime; trained BP neural network models and multiphase correlations can then be selected to estimate the pressure gradients based on the prediction condition. The design of segment-scale estimation of neural network models broadens the prediction range compared to previous designs in the literature and ensures prediction accuracy at the same time by dealing with the problem in a similar way as the finite difference method.

CHAPTER 5

BOTTOM-HOLE PRESSURE CALCULATION RESULTS

Data collected in Table 4.3 was used to test the combined BHP calculation structure developed in this research. The neural network model prediction performance is compared with multiphase correlations. In order to expedite the testing process, a windows application was written in FORTRAN. Some field data, which is completely independent of the data sets used before, is introduced to validate the statistical results.

5.1 Statistical Test Results of Neural Network Models with Training Data

To test the trained neural network models, first the collected data, where segment-scale training data was generated, is used. The statistical results are compared with those from the eleven multiphase correlations, shown in Table 5.1 and plotted in Figure 5.1 and Figure 5.2. From Table 5.1, we can see the ANN models give the best prediction results with lowest average absolute percent error and standard deviation of absolute percent error. Second to that with lowest average error among the correlations is the Mukherjee and Brill (1985) correlation. The Aziz, Govier and Fogarasi (1972) correlation comes in third. Except the correlations in "Category a" as discussed in Section 2.1, Gray (1978) correlation, Duns and Ros (1963) correlation, and Orkiszewski (1967) correlation were primarily developed for vertical flows, and Dukler et al. (1969) correlation was developed mainly for horizontal flows and Beggs and Brill (1973) correlation, Mukherjee and Brill (1985) correlation and Aziz, Govier and Fogarasi (1972) correlation were developed for inclined wells. Hence, the prediction performances of different correlations can vary with prediction condition, i.e. whether the flow is vertical, horizontal or inclined.

Base on the statistical results and combined BHP calculation procedure, when the prediction condition is within the prediction range of ANN models, the piece-wise calculation will select the ANN models to perform the pressure gradient estimation. Otherwise, the

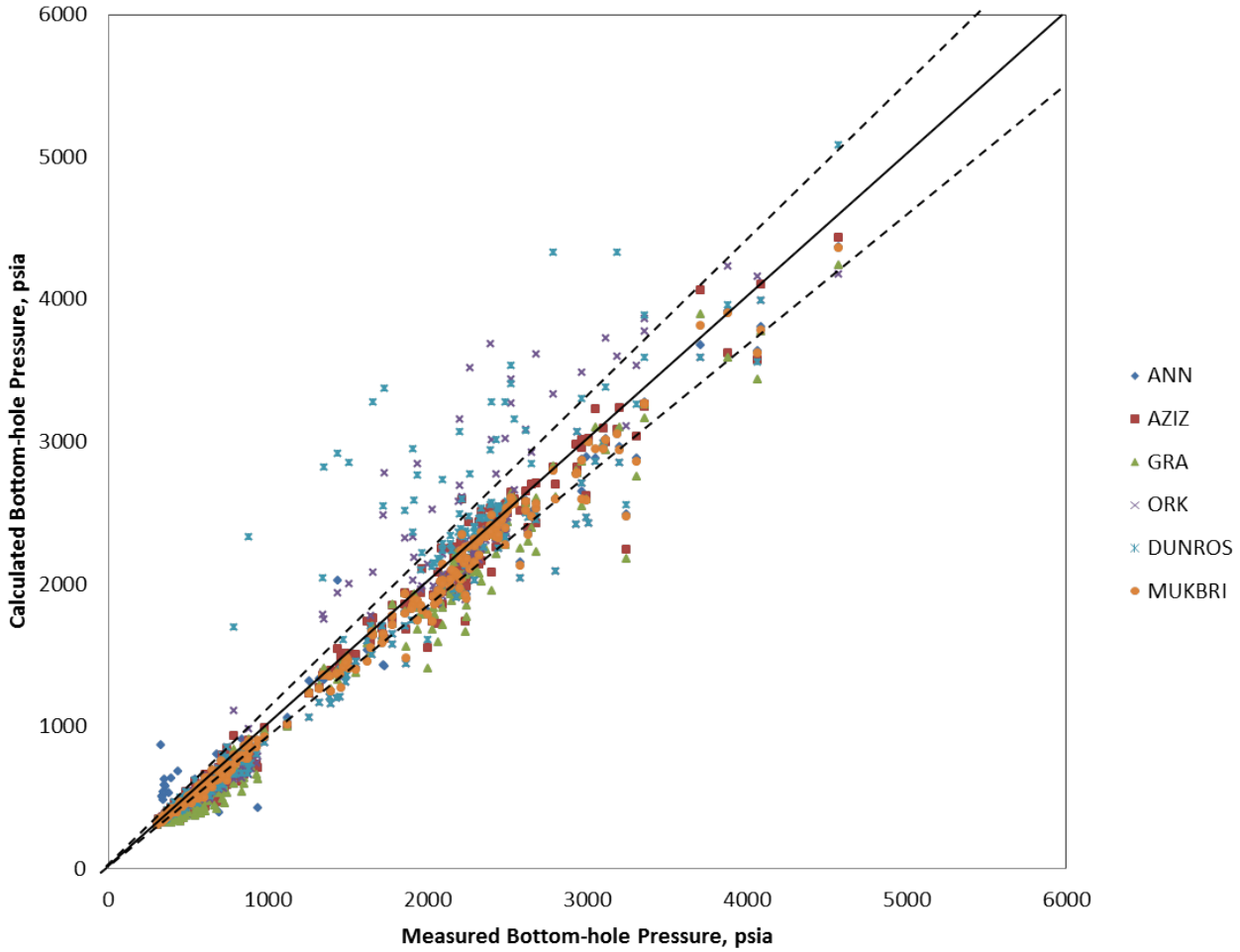

Figure 5.1: The straight solid line indicates that the predicted bottom-hole pressure is equal to actual measurement. The two dashed lines mark the region where predictions within $\pm 10\%$ error lie in. ANN model prediction results follow the solid line except at the low-pressure end. In general, AZIZ and MUKBRI predictions are quite accurate for the whole studied pressure range, while ORK and DUNROS have quite a few predictions significantly off the actual measurements in the higher pressure range. GRA often gives predictions lower than actual values. It should be noted that the abbreviations in the figure are listed in Table 2.1.

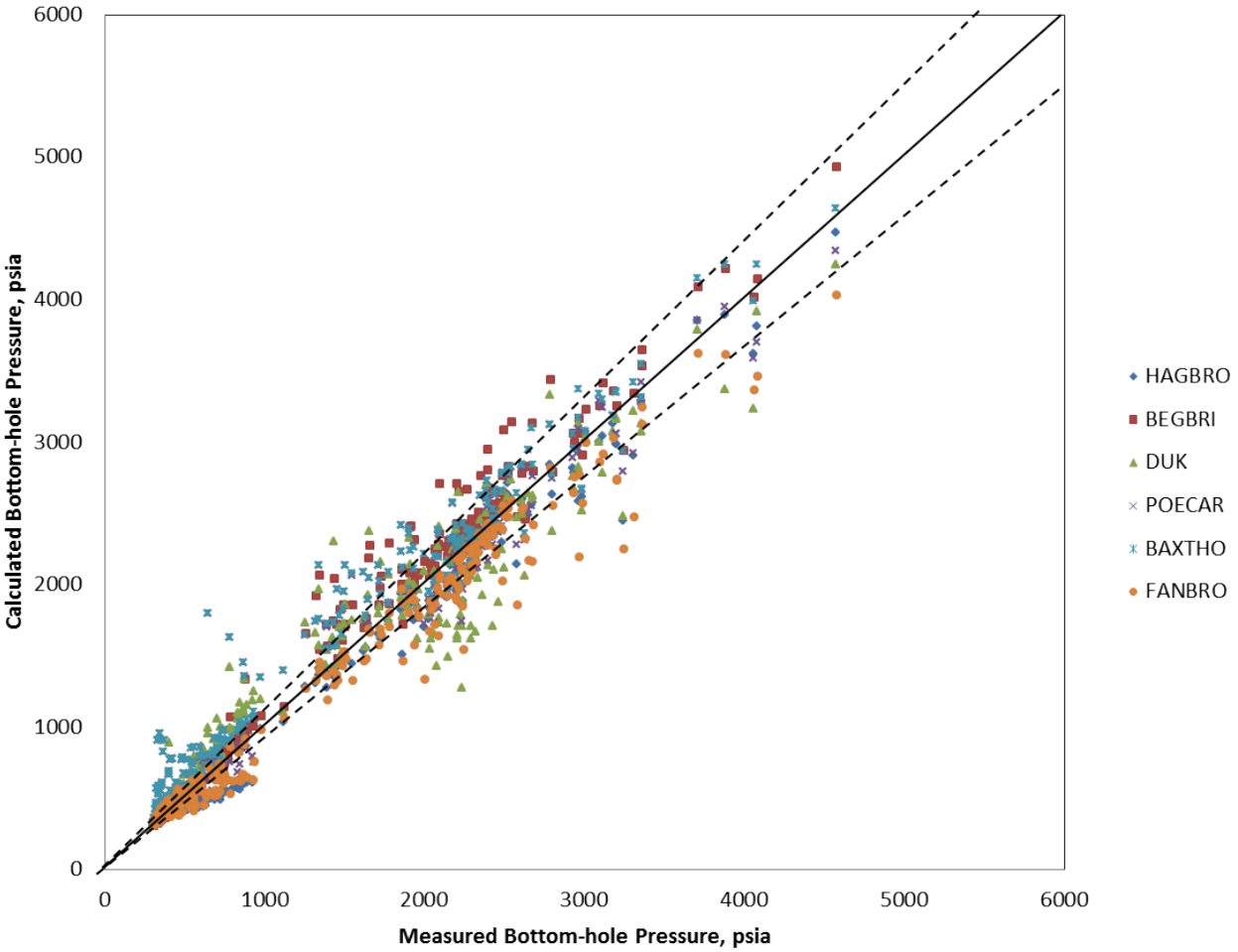

Figure 5.2: BEGBRI, HAGBRO and FANBRO keep most part of the predictions between the two dashed lines which represent errors of $\pm 10\%$. While DUK, POECAR and BAXTHO cannot provide accurate estimations in this case. Comparing to Figure 5.1, the width of the prediction results is wider and the predictions falling exactly on the solid line is less dense, which means that even if the average percent error is low, only a few predictions are very accurate. It should be noted that the abbreviations in the figure are listed in Table 2.1.

Table 5.1: Statistical Results Comparison between ANN models and Multiphase Correlations

Method	Average Absolute Percent Error	Standard Deviation
ANN models	3.1%	0.034
Poettman and Carpenter (1952)	15.4%	0.238
Baxendell and Thomas (1961)	15.5%	0.239
Fancher and Brown (1963)	6.9%	0.073
Hagedorn and Brown (1965)	7.4%	0.087
Gray (1978)	7.5%	0.081
Dukler et al. (1969)	9.0%	0.110
Duns and Ros (1963)	8.2%	0.159
Orkiszewski (1967)	6.6%	0.092
Beggs and Brill (1973)	5.5%	0.077
Mukherjee and Brill (1985)	3.5%	0.038
Aziz, Govier and Fogarasi (1972)	4.8%	0.062

Mukherjee and Brill (1985) correlation will be picked up if the situation is not suitable for ANN models, such as bubble flow and stratified flow, which do not have corresponding ANN models in this study. It should be noted that some other multiphase correlations may work better than the Mukherjee and Brill (1985) correlation under the conditions where ANN models are not suitable. However, due to insufficient data available, the Mukherjee and Brill (1985) correlation will be the only one chosen under those circumstances.

5.2 Multiphase Flow Bottom-hole Pressure Calculator

To implement the research results in this thesis work and facilitate future field application, a windows application, the Multiphase Flow Bottom-hole Pressure Calculator, was developed. The application provides a user-friendly interface, which consists of three tab controls, “INPUT” tab, “SELECT” tab, and “RUN” tab.

On the “INPUT” tab, the required information should be entered into the text boxes according to the units on the right of the boxes. An example is provided to the user to have a better idea of what input values should look like by clicking on the “Show Example” button in the red box, shown in Figure 5.3.

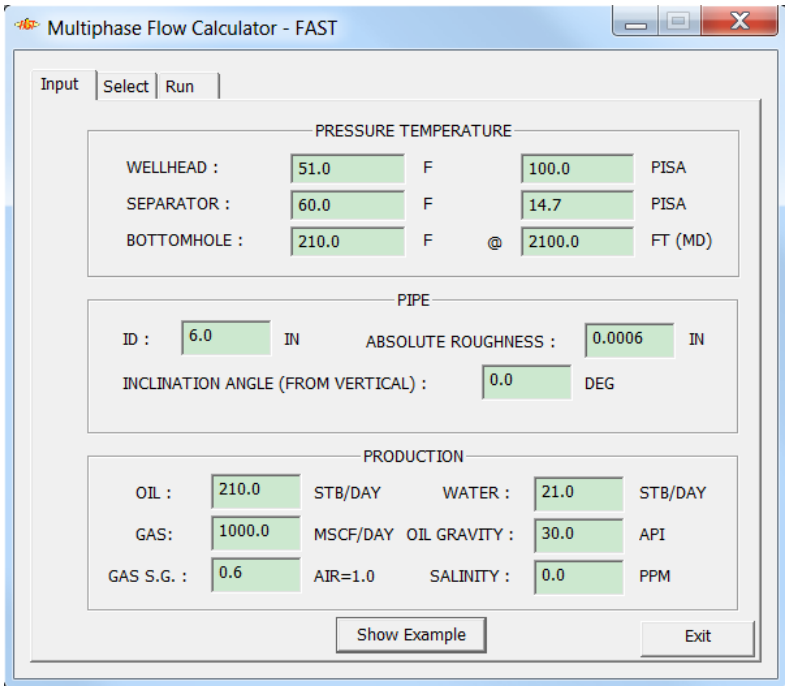

Figure 5.3: Input tab for user to input required measurements for the BHP calculation. The descriptions on the input variables are included in Appendix B.

On the "SELECT" tab, there will be a recommended correlation or method in the line of "RECOMMENDATION: " based on the combined calculation procedure, shown in Figure 5.4. Or users can select their own preferred correlation or method in the dropdown list. After a correlation or method is chosen, the name will be shown after "CHOSEN:".

On the "RUN" tab, the user can click the "RUN" button to trigger the calculation using the method selected on the "SELECT" tab, as shown in Figure 5.5. Two files, one data file and one csv file, will be generated in the same folder where this application is located. The data file contains the input information input from the "INPUT" tab and the csv file has all the intermediate results during the BHP calculation. Main results will be shown, including the calculated bottom-hole pressure in *psia* with the measured depth of bottom-hole, and the estimated measured depth of the fluid level.

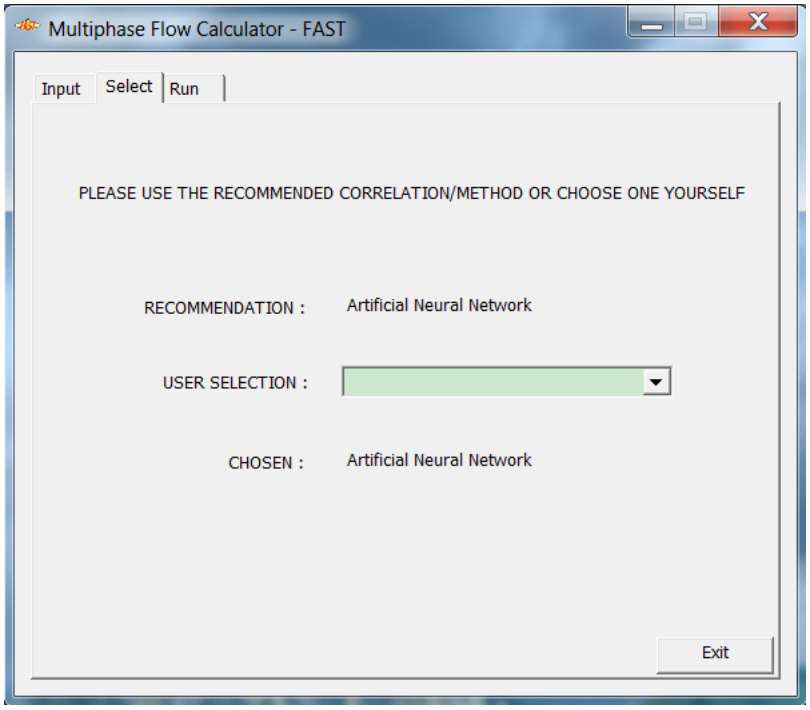

Figure 5.4: Choose the correlation or method for BHP calculation on the "SELECT" tab.

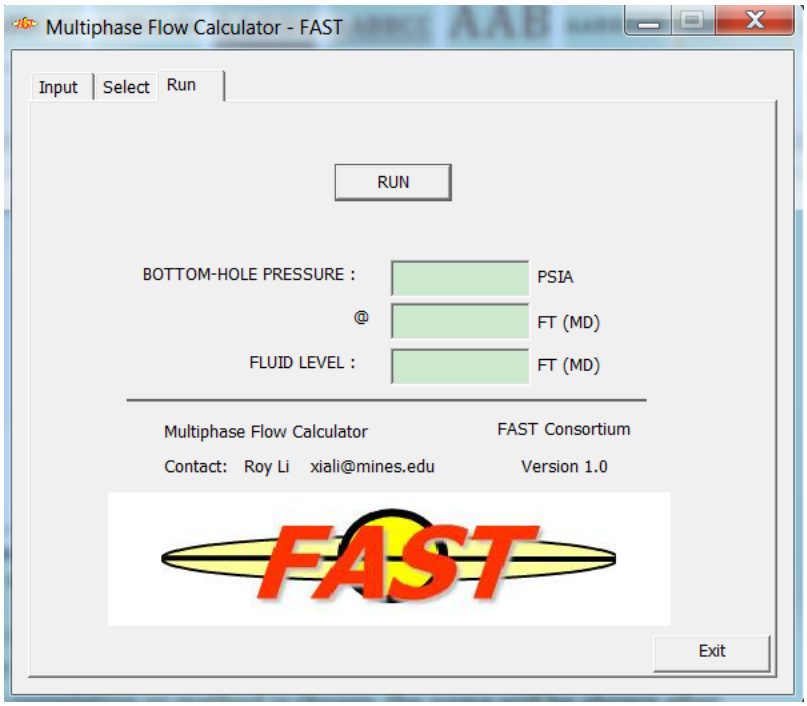

Figure 5.5: Run the BHP calculation from the "RUN" tab.

5.3 Field Data Validation

Extrapolations of the prediction range is always an important aspect for all prediction methods. This combined procedure adopts the piece-wise calculation to broaden its prediction range. To test the prediction accuracy of neural network models under the conditions beyond the condition range of training data sets, some field data from completely independent sources are introduced to the procedure and the calculation results are compared with the actual measurements. The field data was collected from fifteen production wells, which are all gas wells with some water and/or oil production. Average prediction errors are shown in Table 5.2. The results from the eleven multiphase correlations are included as well. The Gray (1978) correlation gives the lowest average error in this case, probably because it was developed specially for vertical gas production well. However, the ANN models, Beggs and Brill (1973) and Mukherjee and Brill (1985) correlations are all proved to have fairly accurate results. It should be noted that some part of the field data was missing, which may affect the comparison results, such as wellhead temperature, which was back-calculated using a geothermal gradient. All the data was found and selected from the production logging file and the measurements might be taken at different times. No indication that the flow is stable when the values were being read. Hence, the average errors of all the methods are generally large in this case, but can still be helpful to evaluate the prediction performance of the different methods. The comparisons between the prediction values and actual values are plotted in Figure 5.6. It is no wonder that the correlations in "Category a" have so large prediction errors due to too much assumptions in the correlations. The Dukler et al. (1969) correlation may not be suitable to predict pressure drops for vertical wells, because it was primarily developed for horizontal flows.

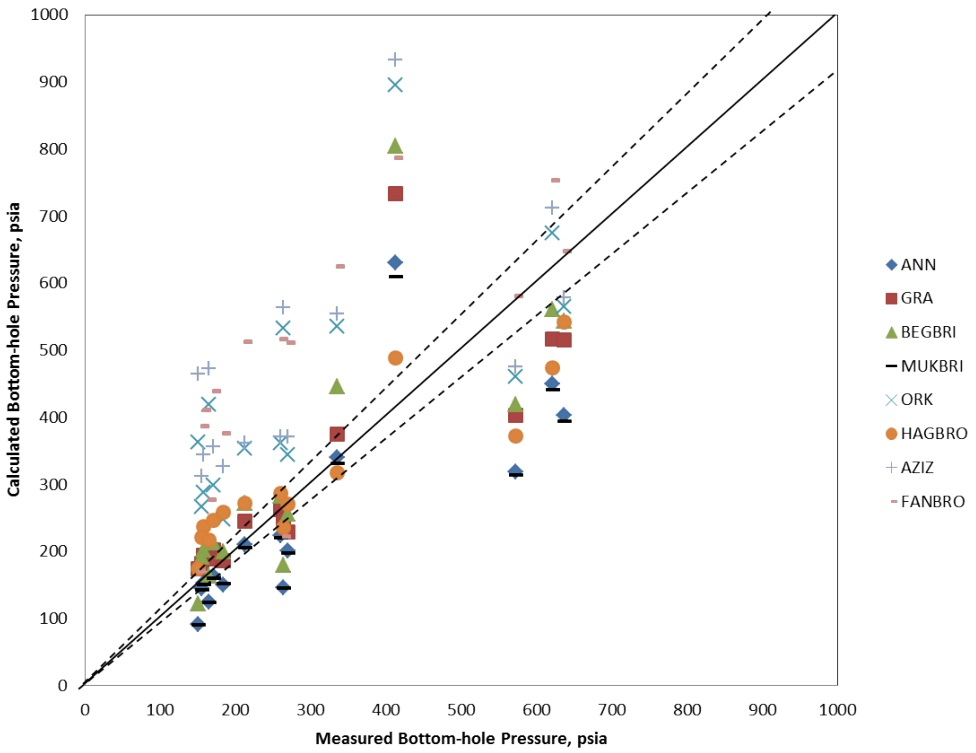

Figure 5.6: The straight solid line indicates that the predicted bottom-hole pressure is equal to actual measurement. The two dashed lines mark the region where predictions within $\pm 10\%$ error lie in. Even though the results from POECAR, BAXTHO, DUK and DUNROS are not included due to the poor predictions, the results shown in the plot are barely satisfactory. However, some predictions do match the actual values quite well for some of the wells and fall exactly on the solid line. It should be noted that the abbreviations in the figure are listed in Table 2.1.

Table 5.2: Field Data Validation Results

Method	Average Absolute Percent Error	Standard Deviation
ANN models	23.0%	0.176
Poettman and Carpenter (1952)	741.0%	4.949
Baxendell and Thomas (1961)	741.0%	4.949
Fancher and Brown (1963)	80.0%	0.578
Hagedorn and Brown (1965)	24.7%	0.156
Gray (1978)	18.8%	0.179
Dukler et al. (1969)	133.3%	1.188
Duns and Ros (1963)	146.8%	2.005
Orkiszewski (1967)	67.3%	0.457
Beggs and Brill (1973)	23.8%	0.222
Mukherjee and Brill (1985)	23.2%	0.170
Aziz, Govier and Fogarasi (1972)	86.5%	0.597

CHAPTER 6

DISCUSSION

It is important to be able to accurately estimate bottom-hole pressure without actually deploying a pressure gauge down the hole. Known parameters used to solve unknown BHP normally include surface measurements, well pipe information, and bottom-hole temperature (can be approximated by reservoir temperature). Many approaches have been developed to solve the multiphase flow problem in between the known and the unknown, including multiphase correlations, mechanistic modeling, and artificial neural network techniques (or artificial intelligence). However, the variation or range of these known input parameters can be too wide for those correlations or methods to handle. Some may work well under certain conditions, and others may not. There is no one single approach that outperforms all others. Results from some papers share the common point that artificial neural network techniques prove to be better tools to deal with multiphase flow problems than traditional approaches, such as correlations and mechanistic modeling (Ternyik et al., 1995, Shippen and Scott, 2002, Osman, 2004, Osman, Ayoub and Aggour, 2005, Ozbayoglu and Ozbayoglu, 2007, Mohammadpoor et al., 2010, Ashena et al., 2010, Al-Shammari, 2011). But still, even with ANN options, the limitations of prediction range remain.

The idea of developing a combined BHP calculation procedure was developed after a careful review of the logic of multiphase correlation calculation procedures and the advantage and ability of various artificial neural network models. Moreover, based on the characteristics of flow regime maps and the features of Support Vector Machine model, a robust SVM model was built to aid flow regime prediction. These two approaches on BHP estimation and flow regime recognition compose the main parts of this thesis. A brief discussion on these two components follows.

6.1 Flow Regime Recognition

It was shown that the gas velocity number, liquid velocity number and inclination angle all matter to multiphase flow regime transitions. However, it was also observed that other variables may change the shape of flow regimes on the map, such as liquid viscosity (Mukherjee, 1979). For example, a higher liquid viscosity tends to be favorable to the formation of larger bubbles, resulting in transition to slug flow at lower gas velocity numbers from bubble flow. Another flaw of the flow pattern map method is the hysteresis effects of liquid and gas flow rates that increasing liquid rate of stratified flow shifts the downhill bubble-stratified flow transition to a higher liquid rate and vice versa (Mukherjee, 1979). Moreover, flow pattern maps are based on experimental observations but don't exactly follow the observations. Besides experimental error, manually drawn lines and equation-fitting error can add to the total prediction error. While support vector machine models are similar but are not limited to a representation of the experimental data without having to impose transition line and fitting equations. As long as test data falls in the condition range of the training data set, SVM models can provide accurate results based on training data and perform interpolation to predict flow regimes for conditions where no training data exists. As for the hysteresis phenomenon of downhill bubble-stratified flow transition, the multiphase pipe flow in actual fields is commonly uphill and/or horizontal.

Another point on the SVM model developed in this study is that due to lack of experimental data, some synthetic data was added to the training data set. Due to time limitations, some available tools were used to train the model but not to fully optimize the model. Hence, should more experimental data and time be given, a more accurate and robust model could be trained.

An interesting phenomenon frequently observed in some cases is the flow regime transition in-between the well. A gas-liquid mixture flows from the formation through the bottom-hole up to the wellhead in the pipe, experiencing temperature and pressure changes throughout the entire system. As pressure decreases, gas in-situ volumetric flow rate increases and the

flow regime may transition from bubble flow to slug flow or from slug flow to mist flow. This change can be important to gas well production. Because of the high initial reservoir pressure, the initial flow in the pipe can be single gas flow or mist flow with gas phase as the continuous phase. During production, with reservoir pressure decreasing and more formation water being produced, the pipe flow may transition to slug flow or even bubble flow. The gas production rate decreases significantly and the well can totally shut down. Therefore, knowing or having the ability to predict when gas phase discontinues being the continuous phase is of importance. On the "RUN" tab of the calculator application, there is a fluid level text box showing the current depth where the continuous phase changes from gas phase. This is calculated as the depth where the predicted flow regime is single gas flow or mist flow on the previous well segment and not on the current well segment in the piece-wise calculation. If the calculation fluid level is above bottom-hole, it seems to be the time to take measures to increase flowing pressure, such as pipe reconfiguration to smaller diameter. Monitoring the fluid level, alerting to changes and taking precautions can help optimize gas production.

6.2 Bottom-hole Pressure Estimation

Before artificial neural network models were introduced to bottom-hole pressure estimation problems, there were two major approaches, including empirical correlations and mechanistic modeling. Due to the vast complexity of multiphase flow compared with single phase flow, empirical correlations were developed to link measurable known variables to pressure gradients based on experimental or field data. Correlations evolve as new features are added in, such as slip effects and flow regime, while mechanistic modeling abandons the empiricism and tries to describe multiphase flow mechanisms physically. However, because there are still too many unknowns and actual conditions can vary, these two approaches can only remain accurate under certain ranges. Attempts to introduce ANN to BHP calculations appear to be rather successful with better or at least not worse performance than those two previous approaches. But an ANN model can be more accurate and robust by improving

the way it is implemented.

The previous work using ANN to calculate BHP all take a one-time estimation, basically taking known variables as model inputs and bottom-hole pressure as the model output. However, by looking over the strategy of piece-wise calculation of multiphase correlations, one can realize that it will be a better implementation if an ANN model is dealt with in a similar way. A one-time estimation is like an average value over the entire well length and can be unreliable especially for deeper wells. Breaking down the total well length into segments, performing a pressure gradient estimation on each segment and adding up the pressure drops on all segments with wellhead pressure to bottom-hole pressure is similar to the finite-difference method in reservoir simulation and should be closer to the actual value than a simple averaging.

Moreover, the piece-wise structure and prediction-condition based method-selection make the combined procedure compatible with complex well trajectory, such as varying inclination angles along the wellbore. This feature has been added into the developed calculator.

One of the major concerns of BHP estimation methods is extendability, i.e. what is the condition range within which this method can give a confident estimation? Performing calculations on segment-scale lengths in the ANN model implementation no longer focuses on total well depth but the variable values on small segments. This smaller segment scale calculation is comparable and universal for any BHP estimation in any case. Therefore, ANN models developed based on the data from one well are safe to be used to calculate pressure gradients in another well, because of this comparability. The possible concern while using the models can be that since some of training data comes from experimental data under laboratory conditions, scaling experimental results up to field conditions may cause some errors.

Another factor that can cause errors to the BHP calculation is the petrophysical correlations. Some of the model input variables, such as viscosity and density, are calculated by petrophysical correlations, as described in Table 4.1. This can produce some error compared

to the actual fluids properties. Especially for gas wells, whether the gas is vaporized from gas condensate or liberated from oil can make big differences in the gas property calculations. There is no clear distinction between these two different types of gases in this study. However, since this study only takes data samples from the results of the most accurate correlations in each case, even if there is no way to prove that each segment result is perfect, the final result, predicted bottom-hole pressure, should be reasonably accurate. Although it is not quite convincing and overlooks validating the individual segment results, it is the only approach available and the results are promising.

At last, we can see that flow regime prediction determines which ANN model should be picked to estimate BHP. This study only used the flow regime transition criteria of Mukherjee and Brill (1985) correlation and not the combination of SVM models and ANN models which would cost considerable time and efforts to finish but which could be a potential direction of extended study in the future.

CHAPTER 7
CONCLUSIONS AND RECOMMENDATIONS

This study of bottom-hole pressure estimation using multiphase correlations and artificial neural network techniques has led to some conclusions as follows:

1. A bottom-hole pressure calculation procedure combining multiphase correlations and artificial neural network techniques was developed. The previous artificial neural network design of a one-time estimation to predict bottom-hole pressure was abandoned in the combined procedure. Instead, different neural network models corresponding to different flow regimes were fitted into the piece-wise calculation procedure of multiphase correlations to increase prediction accuracy and broaden the prediction range.

2. A back-propagation (BP) neural network was used as a pressure gradient prediction model. The model input variables include inclination angle, liquid superficial velocity, gas superficial velocity, gas-liquid surface tension, liquid density, specific gravity of free gas, liquid viscosity, gas viscosity, average pressure, and average temperature. The only output variable is pressure gradient.

3. The BP models adopt an tree-layer structure. The optimization method of Genetic Algorithm was used to help determine the suitable number of neurons on the hidden layer. Two pressure gradient prediction models were trained for slug flow and mist flow.

4. A support vector machine (SVM) flow pattern prediction model was trained in this study. The model takes liquid and gas velocity numbers as input variables and also includes inclination angle effect (from horizontal to upward vertical). Four flow patterns are considered, including bubble flow, slug flow, annular mist flow and stratified flow.

5. Compared with traditional flow pattern map methods to predict flow patterns, support vector machine models are entirely based on actual measurements and avoid the errors from imposing transition lines and fitting equations to the various flow pattern areas.

6. The support vector machine model is like but not limited to a representation of actual data sets. It has interpolation ability to predict flow regimes where no actual data sets exists. The model outputs 3-D plots for all the possible flow patterns at all inclination angles within the studied condition ranges.

7. The collected bottom-hole pressure data samples were used to test the combined procedure. The statistical results show that the combined procedure outperforms all the studied multiphase correlations with the lowest average absolute percent error of 3.1% and standard deviation of 0.034. Second to that is Mukherjee and Brill (1985) correlation with an average absolute percent error of 3.5% and a standard deviation of 0.038.

8. Based on the statistical results, when the prediction condition is within the prediction range of ANN models, the piece-wise calculation will select the developed ANN models to perform the pressure gradient estimation. Otherwise, the Mukherjee and Brill (1985) correlation will be initiated.

9. Some independent field data from the model training data was used to test the combined procedure. The results showed that combined procedure gave fairly accurate predictions with an average absolute percent error of 23.0% and a standard deviation of 0.176. The most accurate correlation in this case, Gray (1978) correlation, predicted the results with an average absolute percent error of 18.8% and a standard deviation of 0.179.

10. To facilitate field application, a Windows application with user graphic interface was written.

Also, some recommendations are made for possible extended study.

1. Because the SVM model was trained using available tools without optimization and some synthetic data was added into the training data sets, the model can be more accurate and robust with more experimental data and further optimization.

2. The SVM model can be extended by exploring possible factors that can affect flow regime transition besides liquid and gas velocity numbers and inclination angle and adding them into the model.

3. Collect more experimental or field data to train BP models for bubble flow and stratified flow to broaden the prediction range of the combined procedure.

4. Since this study only adopted a three-layer BP neural network model structure, a study using multiple hidden-layer structures should be conducted to construct more accurate models.

5. Fully integrate artificial neural network models with multiphase correlation calculation procedures by replacing flow regime criteria of correlations with an SVM model.

6. Further investigate the validity of BP models by sensitivity analysis and comparing with experimental data.

7. The selection of correlations under the conditions off the prediction range of BP models should be studied and added to the combined procedure.

8. A data bank should be established to collect new data to broaden the prediction range of combined procedure. The selection criteria of combined procedure should also be updated every time after new ANN models are trained using updated data bank.

REFERENCES CITED

Abdul-Majeed, Ghassan H and Nimat B Abu Al-Soof. 2000. "Estimation of gas–oil surface tension." *Journal of Petroleum Science and Engineering* 27(3–4):197–200.

Al-Shammari, Ahmed. 2011. Accurate Prediction of Pressure Drop in Two-Phase Vertical Flow Systems using Artificial Intelligence. Society of Petroleum Engineers.

Asheim, Harald. 1986. "MONA, An Accurate Two-Phase Well Flow Model Based on Phase Slippage." *SPE Production Engineering* 1(3):221–230.

Ashena, Rahman, Jamshid Moghadasi, Ali Ghalambor, Mahmood Bataee, Rahim Ashena and Amir Feghhi. 2010. Neural Networks in BHCP Prediction Performed Much Better Than Mechanistic Models. Society of Petroleum Engineers.

Aziz, Khalid, George Govier and Maria Fogarasi. 1972. "Pressure Drop In Wells Producing Oil And Gas." *Journal of Canadian Petroleum Technology* 11:38.

Baker, O.B. and W. Swerdloff. 1956. "Finding Surface Tension of Hydrocarbon Liquids." *Oil and Gas Journal* p. 125.

Barnea, D. 1987. "A unified model for predicting flow-pattern transitions for the whole range of pipe inclinations." *International Journal of Multiphase Flow* 13(1):1–12.

Barnea, Dvora, Ovadia Shoham and Yehuda Taitel. 1982. "Flow pattern transition for vertical downward two phase flow." *Chemical Engineering Science* 37(5):741–744.

Baxendell, P.B. and R. Thomas. 1961. "The Calculation of Pressure Gradients In High-Rate Flowing Wells." *Journal of Petroleum Technology* 13(10).

Beggs, D.H. and J.P. Brill. 1973. "A Study of Two-Phase Flow in Inclined Pipes." *Journal of Petroleum Technology* 25(5).

Beggs, H.D. and J.R. Robinson. 1975. "Estimating the Viscosity of Crude Oil Systems." *Journal of Petroleum Technology* 27(9).

Brill, J. P. and H. Mukherjee. 1999. *Multiphase Flow in Wells*. Vol. 17 of *Monograph Series* Richardson, TX: SPE.

Brill, James P and H. Dale Beggs. 1979. *Two-phase flow in pipes*. Tulsa, Oklahoma: University of Tulsa.

Brinkman, H. C. 1952. "The Viscosity of Concentrated Suspensions and Solutions." *The Journal of Chemical Physics* 20(4):571–571.

Chang, Chih-Chung and Chih-Jen Lin. 2011. "LIBSVM: A library for support vector machines." *ACM Trans. Intell. Syst. Technol.* 2(3):27:1–27:27.

Colebrook, C. F. and C. M. White. 1937. "Experiments with Fluid Friction in Roughened Pipes." *Proceedings of the Royal Society of London. Series A - Mathematical and Physical Sciences* 161(906):367–381.

Colebrook, C.F. 1939. "Turbulent Flow in Pipes, with Particular Reference to the Transition Between the Smooth and Rough Pipe Laws." *J. Inst Civil Eng.* 11:133–136.

Cortes, Corinna and Vladimir Vapnik. 1995. Support-Vector Networks. In *Machine Learning*. Vol. 20 p. 273–297.

Culberson, O.L. and J.J. McKetta. 1951. "Phase Equilibria in Hydrocarbon-Water Systems III - The Solubility of Methane in Water at Pressures to 10,000 PSIA." *Journal of Petroleum Technology* 3(8).

Dranchuk, P. and H. Kassem. 1975. "Calculation of Z Factors For Natural Gases Using Equations of State." *Journal of Canadian Petroleum Technology* .

Dukler, A. E., M. Wicks, O. Baker, M.G. Hubbard and R. G. Cleveland. 1969. *Gas-Liquid Flow in Pipelines, I. Research Results*. New York: AGA-API Project NX-28.

Dukler, A. E., Moye Wicks and R. G. Cleveland. 1964. "Frictional pressure drop in two-phase flow: B. An approach through similarity analysis." *AIChE Journal* 10(1):44–51.

Duns, H. and N. C. J. Ros. 1963. Vertical flow of gas and liquid mixtures in wells. In *6th World Petroleum Congress*. Frankfurt am Main, Germany: World Petroleum Congress.

Eaton, Ben, Charles Knowles and I.H. Silberbrg. 1967. "The Prediction of Flow Patterns, Liquid Holdup and Pressure Losses Occurring During Continuous Two-Phase Flow In Horizontal Pipelines." *Journal of Petroleum Technology* 19(6).

Eaton, Benny Alan. 1966. *The prediction of flow patterns, liquid holdup and pressure losses occurring during continuous two-phase flow in horizontal pipelines, PhD dissertation*. Austin, TX: University of Texas at Austin.

El-Sebakhy, Emad, Tarek Sheltami, Said Al-Bokhitan, Yasser Shaaban, Putu Raharja and Yaman Khaeruzzaman. 2007. Support Vector Machines Framework for Predicting the PVT Properties of Crude-Oil Systems. Society of Petroleum Engineers.

Fancher, George and Kermit Brown. 1963. "Prediction of Pressure Gradients for Multiphase Flow in Tubing." *Society of Petroleum Engineers Journal* 3(1).

Flanigan, O. 1958. "Effect of uphill flow on pressure drop in design of two-phase gathering systems." *Oil and Gas Journal* 56(10):132.

Gaither, Orville, Herald Winkler and C.V. Kirkpatrick. 1963. "Single-and Two-Phase Fluid Flow in Small Vertical Conduits Including Annular Configurations." *Journal of Petroleum Technology* 15(3).

Gould, Thomas. 1974. "Vertical Two-Phase Steam-Water Flow in Geothermal Wells." *Journal of Petroleum Technology* 26(8).

Gould, Thomas, M. Tek and Donald Katz. 1974. "Two-Phase Flow Through Vertical, Inclined, or Curved Pipe." *Journal of Petroleum Technology* 26(8).

Govier, G. W., G. A. Sullivan and R. K. Wood. 1961. "The upward vertical flow of oil-water mixtures." *The Canadian Journal of Chemical Engineering* 39(2):67–75.

Gray, H. E. 1978. "Vertical Flow Correlation - Gas Wells." *User Manual for API 14B, Subsurface Controlled Safety Valve Sizing Computer Program, App. B* pp. 38–41.

Griffith, P. and G. B. Wallis. 1961. "Two-Phase Slug Flow." *Journal of Heat Transfer (U.S.)* Vol: 83.

Hagan, Martin T, Howard Demuth and Mark H. Beale. 1996. *Neural network design*. Boston, MA: PWS Pub. Co.

Hagedorn, Alton and Kermit Brown. 1965. "Experimental Study of Pressure Gradients Occurring During Continuous Two-Phase Flow in Small-Diameter Vertical Conduits." *Journal of Petroleum Technology* 17(4).

Hall, K.R. and L. Yarborough. 1973. "A New Equation of State for Z-Factor Calculations." *Oil and Gas Journal* pp. 82–85, 90, 92.

Hall, K.R. and L. Yarborough. 1974. "How to Solve Equation of State for Z-Factors." *Oil and Gas Journal* pp. 86–88.

Hough, E.W., M.J. Rzasa and B.B. Wood. 1951. "Interfacial Tensions at Reservoir Pressures and Temperatures; Apparatus and the Water-Methane System." *Journal of Petroleum Technology* 3(2).

Jahanbakhshi, Reza, Reza Keshavarzi, Mahdi Aliyari Shoorehdeli and Abolqasem Emamzadeh. 2012. "Intelligent Prediction of Differential Pipe Sticking by Support Vector Machine Compared With Conventional Artificial Neural Networks: An Example of Iranian Offshore Oil Fields." *SPE Drilling & Completion* 27(4).

Katz, D.L. 1942. Prediction Of The Shrinkage Of Crude Oils. Drilling and Production Practice, API p. 137.

Lasater, J.A. 1958. "Bubble Point Pressure Correlation." *Journal of Petroleum Technology* 10(5).

Lee, Anthony, Mario Gonzalez and Bertram Eakin. 1966. "The Viscosity of Natural Gases." *Journal of Petroleum Technology* 18(8).

Mandhane, J.M., G.A. Gregory and K. Aziz. 1974. "A flow pattern map for gas—liquid flow in horizontal pipes." *International Journal of Multiphase Flow* 1(4):537–553.

Mitchell, Melanie. 2002. *An introduction to genetic algorithms*. Cambridge, Mass.: MIT Press.

Mohammadpoor, Mehdi, Khalil Shahbazi, Farshid Torabi and Ali Reza Qazvini. 2010. A New Methodology for Prediction of Bottomhole Flowing Pressure in Vertical Multiphase Flow in Iranian Oil Fields Using Artificial Neural Networks (ANNs). Society of Petroleum Engineers.

Moody, L. F. 1944. "Friction factors for pipe flow." *Trans. ASME* 66(8):671–677.

Mukherjee, H. 1979. *An experimental study of inclined two-phase flow, PhD dissertation*. Tulsa, Oklahoma: University of Tulsa.

Mukherjee, H. and J. P. Brill. 1985. "Pressure Drop Correlations for Inclined Two-Phase Flow." *Journal of Energy Resources Technology* 107(4):549–554.

Nazari, Siamak, Heidi A. Kuzma and James W. Rector. 2011. Predicting Permeability From Well Log Data And Core Measurements Using Support Vector Machines. San Antonio, Texas: 2011 Society of Exploration Geophysicists pp. 2004–2008.

Orkiszewski, J. 1967. "Predicting Two-Phase Pressure Drops in Vertical Pipe." *Journal of Petroleum Technology* 19(6):829.

Osman, El-Sayed A. 2004. "Artificial Neural Network Models for Identifying Flow Regimes and Predicting Liquid Holdup in Horizontal Multiphase Flow." *SPE Production & Facilities* 19(1).

Osman, El-Sayed A., Mohammed A. Ayoub and Mohamed A. Aggour. 2005. Artificial Neural Network Model for Predicting Bottomhole Flowing Pressure in Vertical Multiphase Flow. Society of Petroleum Engineers.

Ozbayoglu, Evren M. and Murat A. Ozbayoglu. 2007. Flow Pattern and Frictional-Pressure-Loss Estimation Using Neural Networks for UBD Operations. Society of Petroleum Engineers.

Peffer, J.W., M.A. Miller and A.D. Hill. 1988. "An Improved Method for Calculating Bottomhole Pressures in Flowing Gas Wells With Liquid Present." *SPE Production Engineering* 3(4).

Poettman, Fred H. and Paul G. Carpenter. 1952. The Multiphase Flow of Gas, Oil, and Water Through Vertical Flow Strings with Application to the Design of Gas-lift Installations. In *Drilling and Production Practice*. American Petroleum Institute p. 257.

Ros, N.C.J. 1961. "Simultaneous Flow of Gas and Liquid As Encountered in Well Tubing." *Journal of Petroleum Technology* 13(10).

Rowe, Allen M. and James C. S. Chou. 1970. "Pressure-volume-temperature-concentration relation of aqueous sodium chloride solutions." *Journal of Chemical & Engineering Data* 15(1):61–66.

Shippen, Mack and Stuart Scott. 2002. A Neural Network Model for Prediction of Liquid Holdup in Two-Phase Horizontal Flow. Society of Petroleum Engineers.

Shoham, Ovadia. 1982. *Flow pattern transition and characterization in gas-liquid two phase flow in inclined pipes, PhD dissertation*. Ramat-Aviv, Israel: Tel-Aviv University.

Standing, M. B. 1947. A Pressure-Volume-Temperature Correlation For Mixtures Of California Oils And Gases. Drilling and Production Practice, API pp. 275–287.

Standing, M. B. 1981. *Volumetric and Phase Behavior of Oil Field Hydrocarbon Systems, ninth printing*. Richardson, TX: Society of Petroleum.

Sutton, Robert. 2007. "Fundamental PVT Calculations for Associated and Gas/Condensate Natural-Gas Systems." *SPE Reservoir Evaluation & Engineering* 10(3).

Sutton, Robert. 2009. An Improved Model for Water-Hydrocarbon Surface Tension at Reservoir Conditions. Society of Petroleum Engineers.

Taitel, Yehuda, Dvora Bornea and A. E. Dukler. 1980. "Modelling flow pattern transitions for steady upward gas-liquid flow in vertical tubes." *AIChE Journal* 26(3):345–354.

Ternyik, J., H.I. Bilgesu, S. Mohaghegh and D.M. Rose. 1995. Virtual Measurement in Pipes: Part 1-Flowing Bottom Hole Pressure Under Multi-Phase Flow and Inclined Wellbore Conditions. Morgantown, WV: Society of Petroleum Engineers.

Van Wingen, N. 1950. *Secondary recovery of oil in the United States.* New York City: American Petroleum Institute.

Vapnik, Vladimir N. 1995. *The nature of statistical learning theory.* New York: Springer.

Vazquez, M. and H.D. Beggs. 1980. "Correlations for Fluid Physical Property Prediction." *Journal of Petroleum Technology* 32(6):968–970.

APPENDIX A - ORIGINAL FLOW PATTERN DATA

The flow pattern data is collected from the thesis experimental work of Mukherjee (1979). A total of 598 measurements are listed in the supplemental file, SVM_flow pattern training data from "SVM_flow pattern training data from Mukherjee.xlsx", listed in Table C.1.

APPENDIX B - DESCRIPTIONS ON THE INPUT DATA ON WINDOWS APPLICATION

The input variables used in Figure 5.3 are described in Table B.1.

Table B.1: Windows Application Input Variable Description

Input Data	Description	Unit
Wellhead Temperature	Temperature measured at the wellhead. It is used to calculate temperature gradient along the well.	°F
Wellhead Pressure	Pressure measured at the wellhead. Starting pressure for the calculation.	psia
Separator Temperature	Temperature at the separator where specific gravity of produced gas is reported. 60 °F for standard condition. It is usually used with separator pressure to convert surface measurements to standard condition.	°F
Separator Pressure	Pressure at the separator where specific gravity of produced gas is reported. 14.7 psia for standard condition.	psia
Bottom-hole Temperature	Temperature measured at bottom-hole. Can be estimated using wellhead temperature and geothermal gradients.	°F
Bottom-hole Measured Depth	The measured depth of bottom-hole. Can be converted to/from true vertical depth using inclination angle.	ft
ID	Inner diameter of well pipe. It affects the superficial velocities and some dimensionless numbers.	inch
Absolute Roughness	Absolute well pipe roughness. A parameter to estimate friction factor.	inch
Inclination Angle	The inclination angle measured from vertical direction. Positive value indicates upward flow; negative value indicates downward flow.	DEG
Oil Production Rate	Oil flow rate measured at standard condition. It is used to calculate liquid superficial velocity.	stb/day
Water Production Rate	Water flow rate measured at standard condition. It is used to calculate liquid superficial velocity.	stb/day
Gas Production Rate	Gas flow rate measured at standard condition. It is used to calculate gas superficial velocity.	Mscf/day
Oil API Gravity	A measurement of oil density or gravity, which is part of liquid density. It is used to calculate many fluid properties, such as oil and gas surface tension, solution gas-oil ratio, bubble point, and formation volume factor.	-
Produced gas Specific Gravity	The ratio of gas density compared to air density at a specified temperature and pressure. It can affect the oil bubble point pressure.	-
Water Salinity	The saltiness or dissolved salt content of a body of water. Usually measured in parts per million. It can affect water gravity and water gas surface tension, but is set as 0 by default.	ppm

APPENDIX C - SUPPLEMENTAL ELECTRONIC FILES

To make this work reproducible, some program code files and data files for training data and test results are provided and recorded on a CD. All the files are described and summarized in Table C.1.

Table C.1: Supplemental Electronic Files

File	Description
Data Files	Files containing training data for support vector machine and back-propagation models.
SVM_flow pattern training data from Mukherjee.xlsx	Support vector machine model training data collected from Mukherjee (1979). N_{gv} (gas velocity number), N_{Lv} (liquid velocity number), θ (inclination angle from horizontal) and flow pattern observation. The numbers in "Flow Pattern" columns indicate the observed flow patterns, including 3 for bubble flow, 4 for slug flow, 5 for annular mist flow, and 6 for stratified flow.
literature_data.xlsx	Well data collected from literature. Used to test multiphase correlations and generate training data for BP models.
Windows Application Code Files	Containing all the source code for the multiphase correlations and artificial neural network models. Resource files, such as icon, dialog drawing files, are not provided.
ANN_MPF.f90	The code file for trained artificial neural network models to estimate pressure gradients.
AZIZ.f90	The code file to perform Aziz, Govier and Fogarasi (1972) correlation calculations.
BAXENDELL_THOMAS .f90	The code file to perform Baxendell and Thomas (1961) correlation calculations.
BEGGS_BRILL.f90	The code file to perform Beggs and Brill (1973) correlation calculations.
DEPTH.CONVERTOR.f90	To perform Lagrangian interpolation among true vertical depth, measured depth and inclination angle.
DUKLER.f90	The code file to perform Dukler et al. (1969) correlation calculations.
DUNS_ROS.f90	The code file to perform Duns and Ros (1963) correlation calculations.

Table C.1: Continued.

File	Description
FANCHER_BRWON.f90	The code file to perform Fancher and Brown (1963) correlation calculations.
FLUIDS_PROPERTIES.f90	Containing all the petrophysical correlations to estimate fluids properties.
GRAY.f90	The code file to perform Gray (1978) correlation calculations.
HAGEDORN_BROWN.f90	The code file to perform Hagedorn and Brown (1965) correlation calculations.
LAGRANGIAN_INTERPOLATION.f90	Can be used to perform Lagrangian interpolation.
MUKHERJEE_BRILL.f90	The code file to perform Mukherjee and Brill (1985) correlation calculations.
ORKISZEWSKI.f90	The code file to perform Orkiszewski (1967) correlation calculations.
POETTMANN_CARPENTER.f90	The code file to perform Poettman and Carpenter (1952) correlation calculations.
Support Vector Machine Model Training Code	Containing all the files used during the support vector machine model training.
data_Kerosene_uphill.mat	Matlab data file containing the input training data for support vector machine.
SVMcgForClass.m	Grid search method for best selection of c and γ model parameters, as discussed in Section 3.2.2.
Train_Kerosene_uphill_Grid_Search.m	Train support vector machine with the data in data_Kerosene_uphill.mat file using Grid search method from SVMcgForClass.m file.